Nanoscale

ROYAL SOCIETY OF CHEMISTRY

REVIEW

View Article Online
View Journal | View Issue

Cite this: *Nanoscale*, 2025, **17**, 12554

Carbon dot–phthalocyanine hybrids: synergistic effects that boost their multifaceted applications

Carla I. M. Santos, *[a,b] Ana Catarina Almeida, [c] Ana L. F. Martins,[c] Ana R. Araújo,[b] Leandro M. O. Lourenço, *[b] Gil Gonçalves *[c,d] and M. Graça P. M. S. Neves *[b]

Received 31st January 2025,
Accepted 8th April 2025

DOI: 10.1039/d5nr00466g

rsc.li/nanoscale

Since their discovery, carbon dots (CDs) have been extensively studied for their potential in diverse applications owing to their unique properties such as high biocompatibility, excellent water solubility, low toxicity, minimal photobleaching, and exceptional chemical versatility. These characteristics position CDs as promising candidates for overcoming the limitations of various molecular compounds. This review provides a comprehensive analysis of the synergistic effects arising from the integration of CDs and phthalocyanines (Pcs) to form hybrids with distinct photophysical and photochemical properties. This study explores recent advances in the development of Pc@CD hybrids, focusing on their synthesis, conjugation strategies, and synergistic effects that impact their performance in several areas, including optical sensing, electrocatalysis, photodynamic processes and photocatalysis. Emphasis is given to chemical methods that enable efficient conjugation and the role of the generation of reactive oxygen species in driving these applications. Additionally, the discussion also addresses key challenges, highlighting innovative solutions and proposing future research directions to fully harness the potential of Pc@CD hybrids in diverse scientific and technological breakthroughs.

1. Introduction

1.1. Carbon dots' structure and properties

Carbon dots (CDs) are considered a new emerging class of zero-dimensional (0D) carbon-based luminescent nanomaterials. Although CDs have just recently gained popularity, it is postulated that they should be one of the oldest and most abundant nanoparticles on the Earth, resulting from natural phenomena such as combustion.[1,2] Their denomination arises from the fact that they are mainly composed of carbon in different types of hybridization states. Typically, CDs present a broad photoluminescence (PL) profile where the emission is extremely dependent on the excitation wavelength. The optical properties of the CDs are usually controlled by intrinsic structural features including the size and morphology, functional groups, and heteroatom doping. CDs are defined by a size below 10 nm with a quasi-spherical morphology, which are composed of an sp^2/sp^3 carbon core that can be easily doped with heteroatoms like boron, nitrogen, and/or sulfur.[3] Their surface usually presents abundant functional groups such as carboxyl, hydroxyl, amine, and/or polymer chains, depending on the raw material and synthesis method applied for their fabrication.[4] Although important pieces of the puzzle about the chemical structure of CDs have been uncovered, some critical knowledge remains unknown, owing to the complexity of the reaction pathways involved in their manufacture.[5] Consequently, the molecular origin and other key factors that control CDs' photophysical properties are still, in most cases, an enigma that has been slowly revealed.[6] So far, it is well known that some properties of CDs can be mainly attributed to their core, such as toxicity, while other properties such as dispersibility and optical properties can be mainly ascribed to their surface functional groups.[7] ^{1}H and ^{13}C nuclear magnetic resonance (NMR) has been recently explored as an essential tool for the identification of the functional groups of CDs, thanks to its accuracy in disclosing molecular species.[8] The impact of CDs on scientific research has been mostly associated with their extraordinary optical properties, including tuneable photoluminescence,[9] excitation wavelength-dependent emission,[10] and multiphoton excitation.[11–13]

The intense research on light-emitting CDs was sparked in 2006 with the discovery of room-temperature light emission.[14] The pioneer CDs presented emissions mostly located in the blue- or green-light region; however, researchers recently devel-

[a]*Centro de Química Estrutural (CQE), Instituto Superior Técnico, Av. Rovisco Pais, 1049-001 Lisboa, Portugal. E-mail: carla.santos@tecnico.ulisboa.pt*
[b]*LAQV-REQUIMTE, Department of Chemistry, University of Aveiro, Campus Universitário de Santiago, 3810-193 Aveiro, Portugal. E-mail: leandrolourenco@ua.pt, gneves@ua.pt*
[c]*TEMA-Nanotechnology Research Group, Mechanical Engineering Department, University of Aveiro, Campus Universitario de Santiago, 3810-193 Aveiro, Portugal. E-mail: ggoncalves@ua.pt*
[d]*Intelligent Systems Associate Laboratory (LASI), 4800-058 Guimarães, Portugal*

oped new synthetic strategies to shift their emission to red- and near-infrared regions (therapeutic window) to improve their relevance for biomedical applications.[15–18] Nowadays, CDs can present a broad range of emission bands covering almost the full spectrum, including UV-Vis and infrared regions.[19–21]

The extensive versatility of chemical modifications in CDs renders them highly desirable for overcoming diverse technological challenges. Several strategies have been employed, including heteroatom[22] or metal[23] surface passivation,[24] edge group modification,[25] or organic functionalization.[6] Compared to heteroatom doping, surface functionalization, based on well-established organic reactions, is more controllable. Various approaches have been explored for the chemical modification of CDs including surface chemistry interactions (*e.g.*, hydrophobic, electrostatic, and π–π interactions) or through the establishment of strong molecular bonds (*e.g.*, covalent bonding and coordination). The chemical surface modification of CDs can contribute to tuning solvents' dispersibility, induce desired biological targeting, regulate catalytic performance, improve the photoluminescence (PL) emission, and regulate the band gaps of CDs. These extraordinary features of CDs allowed their fast proliferation for the development of advanced novel materials that found relevant applications in several fields, including biomedicine, sensing, (photo)catalysis, electronics, energy, and environmental remediation. In addition, CDs present lower toxicity, minor production costs, and excellent biocompatibility when compared with some traditional semiconductor inorganic quantum dots containing cadmium or lead.[26–29]

The extensive diversity of methodologies explored thus far, coupled with the wide array of available carbon-based raw materials, has led to an exponential growth in the preparation of various types of CDs. The categorization of CDs is closely linked to the extent of carbonization and graphitization within their carbon core. Therefore, the synthetic parameters of CDs can be customized to achieve specific properties (Fig. 1A).

Effective control of the experimental parameters is critical for controlling the structure, morphology, and final properties of CDs. The first step in the design of CDs is to properly define the starting materials that can originate from organic or inorganic precursors. Organic precursors, such as citric acid, glucose, or amino acids, tend to produce amorphous or quasi-graphitic CDs, whereas inorganic precursors might result in more graphitic CDs. The temperature at which synthesis occurs can significantly affect the degree of carbonization and graphitization. Higher temperatures often lead to more ordered graphitic structures, whereas lower temperatures induce the formation of amorphous carbon structures. The reaction duration is also an important parameter, with longer reaction times favouring more extensive carbonization and graphitization, resulting in CDs with a higher degree of crystallinity. The type of atmosphere (air, nitrogen, or argon) can also affect the carbonization process, where inert atmospheres such as nitrogen or argon can promote graphitization by minimizing oxidation. The concentration of the precursors, the pH of the reaction solution, and the choice of solvent can influence the reaction kinetics, and consequently, the structure of the CDs. The carbonization process can also be affected by the solvent type. The introduction of dopants or surface functional groups during the synthetic process can further modify the properties of CDs. Post-synthesis treatments, such as annealing or surface passivation, can be applied to modify the properties of CDs after synthesis. The diverse range of CDs reported in recent years has sparked vigorous debates regarding their classification and nomenclature. Consequently, the absence of well-defined parameters for standardization has resulted in similar CDs being referred to by different designations. As a result of this imprecise terminology, distinguishing between different types of CDs in the literature has become a considerable challenge. To address this classification challenge, we will adopt the categorization proposed by Prato *et al.*,[5] which is based on three fundamental criteria: morphology, quantum confinement effects (QCEs), and crystallinity (Fig. 1A). According to this classification, CDs can be divided into four primary subtypes. Graphene quantum dots (GQDs) feature a graphitic planar structure modified with chemical functional groups either at the edges or within interlayer defects. These functional groups are responsible for their intriguing quantum confinement effects and edge effects. GQDs typically have a higher ratio of sp^2 carbon atoms, resembling a few layers of graphene in their core, with the surface covered by sp^3 carbon atoms. Their QCEs are linked to the size of the emissive π domains. The carbon quantum dots (CQDs) exhibit a spherical core–shell morphology, with a crystalline lattice containing a high density of sp^2 hybridized carbon atoms in the core and a shell intercalated typically with oxygen and nitrogen functional groups. These structural features result in quantum confinement effects within the emissive π domains. Carbon nanodots (CNDs) are quasi-spherical nanoparticles characterized by a carbonized core structure and surface functional groups. Carbonized polymer dots (CPDs), typically possessing quasi-spherical morphologies, have hybrid structures comprised of sp^2, sp^3, or both sp^2 and sp^3 hybridized carbon atoms in their core. The surfaces are densely covered with polymer chains, and their photoluminescence properties are primarily attributed to the crosslink-enhanced emission effect. Two major approaches can be found in the literature regarding the preparation of CDs: bottom-up and top-down approaches (Fig. 1A).[5,30–33]

The bottom-up approach typically explores molecular organic precursors, carbohydrates, and polymers as raw materials for the preparation of CDs. Most of the precursors, after being subjected to hydrothermal treatment, microwave (MW)-assisted synthesis, or pyrolysis, undergo partial dehydration and dehydrogenation before forming the CDs' backbone structure.[34–37] Bottom-up methods are typically used to afford CPDs but have also been extensively used to prepare GQDs and CQDs. Usually, the preparation of CDs using this approach requires harsh reaction conditions, such as high temperature and pressure. In addition, it was reported that the addition of other chemical agents to the reaction medium, such as acids,

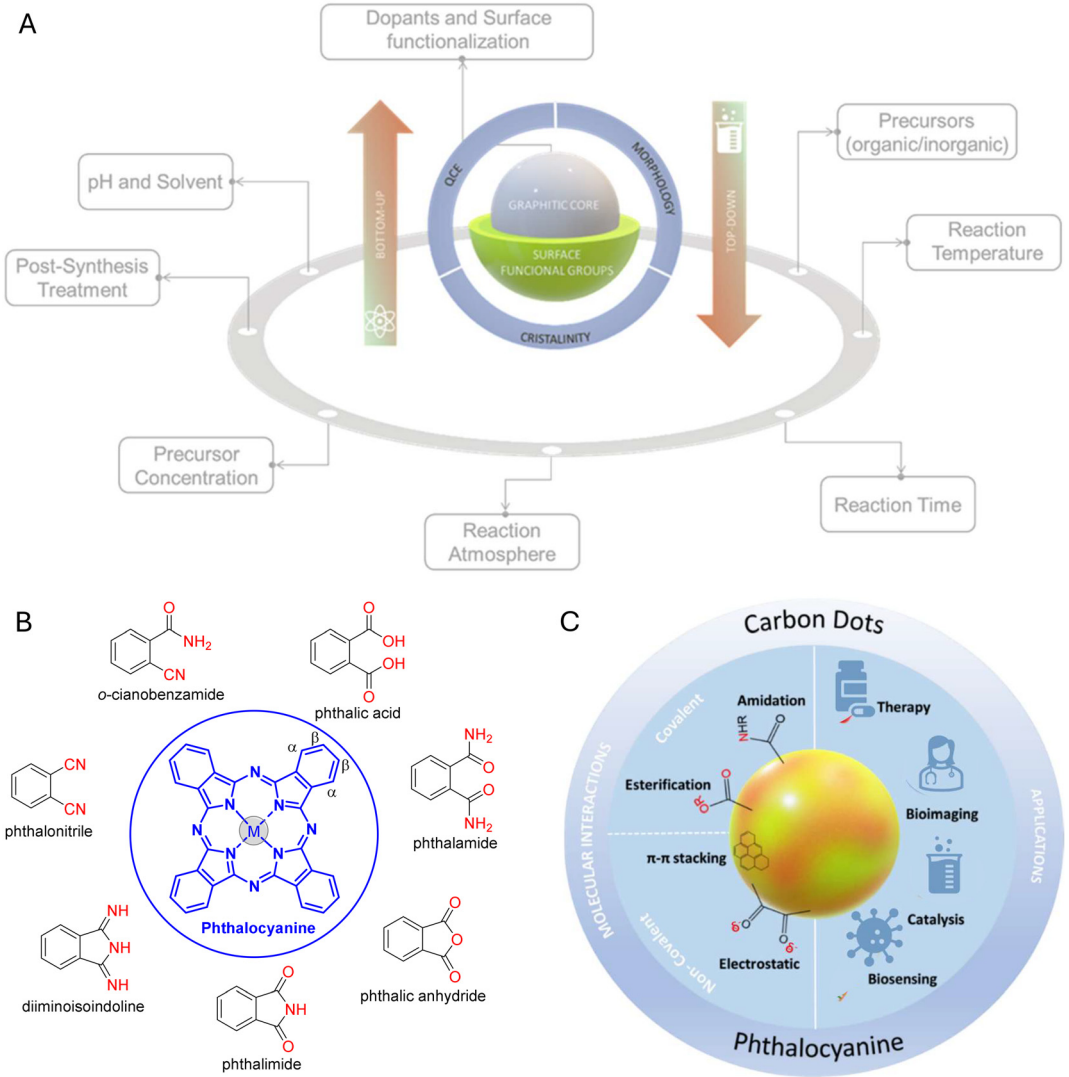

Fig. 1 (A) Key synthetic experimental parameters that influence the chemical, structural and optical properties of CDs. Typical structure of CDs showing the graphitic core and surface functional groups, with an indication of the bottom-up and top-down synthesis. Indication of the main parameters used for CDs' current classification: crystallinity, morphology, and quantum confinement effects (QCEs). (B) Free-base phthalocyanine (M = 2H) and metallophthalocyanine (M = metal ion) structures prepared from the most common precursors. The nomenclature of a phthalocyanine macrocycle is described according to the IUPAC; the letters β and α indicate the peripheral and non-peripheral positions, respectively. (C) Left side: overview of the different molecular interactions of CDs with Pcs, divided into covalent and noncovalent interactions. Right side: overview of different applications of CDs linked to Pcs.

can favor the formation of CDs.[38] The hydrothermal synthesis of CDs using organic precursors in a Teflon-lined autoclave has been one of the most explored bottom-up strategies owing to the simplicity of the experimental protocol. The basic premise of CD formation consists of the reaction between the carbon precursors to form small graphitic structures upon heating. As mentioned above, the size and degree of carbonization of CDs can be effectively controlled by optimizing different reaction parameters, such as solvents, temperature, and reaction time.[39] The most explored precursor for the synthesis of CDs is citric acid (CA), which, in conjugation with different nitrogen-containing precursors, allows obtaining CDs with different optical features in a controlled manner.[40–42]

The top-down approach is characterized by the extensive fragmentation of carbon-based materials, whether they are in macro-, micro-, or nano-form, into tiny nanosized particles. This strategy typically employs carbon allotropes as raw materials, including graphite, carbon black, carbon fibers, carbon nanotubes (CNTs), carbon nanohorns (CNHs), fullerenes, and various graphene-based materials. The primary objective is to convert the large sp^2 carbon domains within these materials into smaller sp^2 domains, ultimately forming GQDs.[13] Consequently, following this conversion process, the inherent zero bandgap of the graphene structure transforms into a nonzero bandgap due to quantum confinement. This transformation was accompanied by an increase in edge

defects, which played a crucial role in the properties of the resulting GQDs. The controlled process of fragmenting graphene can be achieved through several methods, including arc discharge, ball milling, laser ablation, chemical oxidation, and electrochemical etching.[43] In particular, the chemical oxidation of carbon nanostructures using MW or hydrothermal treatment has garnered significant attention for the preparation of GQDs. Among these methods, graphene oxide (GO) derivatives have emerged as a popular choice as precursor materials for the top-down synthesis of GQDs.[44–46] The high oxidation state of GO nanosheets and their derivatives, characterized by randomly dispersed small sp^2 domains within an sp^3 matrix, facilitates efficient chemical nanocutting. This process ultimately results in the formation of oxygen-doped GQD fragments with tunable optical properties.

The chemical structure of CDs plays a crucial role in mediating their functionalization, whether through covalent or non-covalent approaches. As mentioned above, CDs possess various functional groups on their surface, such as amino, hydroxyl, and carboxyl, which improve their water stability and provide ideal sites for functionalization with ions, molecules, biomolecules, and polymers. Among these, amine and carboxyl groups are most commonly used for covalent conjugation with PCs through amide bond formation. The concentration of these functional groups on the CD surface typically determines the success and yield of the reaction. CDs can also undergo additional chemical modifications to increase the density of these functional groups. A common approach involves converting hydroxyl (–OH) groups to carboxyl (–COOH) groups, which is easily implemented through the reaction with chloroacetic acid under basic conditions.[46] Non-covalent conjugation of CDs with PCs is another widely explored approach for the synthesis of novel hybrid materials. The surface functional groups can facilitate electrostatic interactions with positively or negatively charged PCs, depending on the pH of the reaction medium. Another approach relies on π–π stacking or establishing hydrophobic interactions. In contrast to covalent conjugation, where a higher density of surface functional groups is beneficial, non-covalent conjugation is more effective when CDs have lower surface functionalization and larger aromatic domains.[32] Although the aromatic structure of CDs is highly dependent on the synthesis method, various reduction post-treatments have been explored to enhance their graphitic domains, thereby improving their conjugation efficiency with PCs.

However, it is important to note that the chemical structure of PCs can be tuned with complementary functionalization to enhance their covalent or non-covalent interactions with CDs.

1.2. Phthalocyanines' structural features and synthetic approaches

Pcs are a class of macrocycles of synthetic origin that are structurally similar to analogous porphyrin derivatives, but with a core composed of four isoindole units linked through aza-bridges (Fig. 1B). The term "phthalocyanine" (Pc) was suggested by Linstead in 1933 to describe these blue-green pigments and resulted from the combination of the prefix *phthalo*, highlighting their synthetic origin from phthalic anhydride and derivatives, and *cyanine* due to their dominating blue color. However, the first reference to these blue-green derivatives appeared in 1907, when Tcherniac *et al.* noticed the formation of a small amount of a blue compound after heating *o*-cyanobenzamide.[47] In 1927, Von der Weid *et al.* of the University de Fribourg described the formation of a highly stable blue material during the chemical reaction of 1,2-dibromobenzene with copper cyanide in pyridine reflux.[48–50] However, the compound was not correctly identified (molecular formula $C_{26}H_{18}N_6Cu$),[48] and only six years later (1933), Linstead reported the correct structure as the free-base phthalocyanine **H_2Pc** and its Cu(II) complex **CuPc** (Fig. 1B). In the same period, Scottish Dyes Ltd also detected a highly stable and insoluble blue impurity during their attempts to produce phthalimide from phthalic anhydride and ammonia, which was patented due to its economic interest, and was posteriorly identified, namely by X-ray crystallography, as the Fe(II) complex of phthalocyanine.[51–56] With this progress, synthetic routes were reported[57–60] and, in 1935, Cu(II) phthalocyanine was synthesized at an industrial scale and used as a blue pigment in the paint industry. Linstead's investigations were encouraging, but in the case of other scientific areas, the insolubility of these pigments limited their use. In the 60s, the synthesis of highly soluble Pc derivatives allowed the diversification of the applications of these chromophores to other fields.[61–63] In the synthesis of this type of macrocycle, a great variety of precursors can be used, such as *o*-cyanobenzamide, phthalic acid, phthalic anhydride, phthalimide, diiminoisoindoline, and phthalonitrile (Fig. 1B).[61,64] Among the most common precursors are phthalonitriles, which, depending on the reaction conditions (*e.g.*, reaction time, temperature, solvent, type of atmosphere, base, and catalyst selected),[65] are initially transformed into diiminoisoindoline derivatives *via* reaction with ammonia. This is followed by cyclotetramerization, which usually occurs in alcoholic solutions at high temperatures. It is noteworthy that the reaction is favoured by the use of a catalytic amount of organic base, such as 1,8-diazabicyclo[5.4.0]undec-7-ene (DBU) or 1,5-diazabicyclo[4.3.0]non-5-ene (DBN) in pentanol.[66–68] However, reactions with other precursors, such as phthalimide, phthalic acid, and phthalic anhydride, require urea as a nitrogen donor. To prepare free-base Pcs, lithium or magnesium is commonly used as a template, followed by demetallation of the obtained Pc complexes under dilute acidic conditions. On the other hand, the synthesis of metallophthalocyanines (**MPc**, M = metal ion) can involve two different approaches: (i) the metal is inserted directly into the macrocycle during the tetramerization process using a phthalonitrile and an adequate metal salt[69] and (ii) the metal is introduced in the previously prepared free-base **H_2Pc** using an adequate metal salt carrier.[70] In the first approach, access to the metal complexes of Pcs requires the heating of the phthalonitrile derivative with the adequate metallic salt in a solvent with a high boiling point, such as dimethylaminoethanol (DMAE), *N*,*N*′-dimethylformamide (DMF)

or 1-chloronaphthalene.[66] However, some procedures can be carried out at lower temperatures by using a basic catalyst namely DBU in pentan-1-ol[66] or even at room temperature by using lithium in DMAE.[71] These conditions are also relevant for converting **H_2Pcs** adequately substituted at peripheral positions into different **MPcs** (M = Zn^{2+}, Mg^{2+}, In^{3+}, Ga^{3+}, Ge^{3+}, and Si^{4+}, among others). Most Pcs' applications are related to the delocalization of 18 π-electrons, leading to relevant physicochemical and photophysical/photochemical features. In general, their electronic spectra present a broad band at around 300–400 nm called the Soret band (S-band) and an intense Q-band in the range of 600–750 nm. Moreover, the excitation of Pcs at a specific wavelength reveals fluorescence emission between 600 and 800 nm. It is well established that the required features of a Pc for a special target application can be modulated through structural alterations at the peripheral α- and/or β-positions, leading to new systems with distinct characteristics, such as (photo)stability, water solubility, electron transfer abilities, suitable singlet oxygen ($^1O_2$) quantum yields (Φ_Δ), and fluorescence quantum yields (Φ_F). This is responsible for the unequivocal success of Pcs in several scientific areas, namely: (i) biomimetic models of photosynthetic primary processes;[72] (ii) catalysts[73,74] or photocatalysts;[73,75] (iii) sensors;[70,76] (iv) photosensitizers (PSs) for antimicrobial photodynamic therapy (aPDT) under different contexts;[77–80] (v) PSs for photodynamic therapy (PDT) of malignant diseases,[81–83] (vi) G-quadruplex aptamer binding,[84–86] and (vii) markers in photomedicine.[87] More recently, the possibility of combining Pcs with different carbon-based nanostructures (*e.g.*, CNTs, GO, or CDs)[88–90] to develop new conjugates with improved features for different applications has been an important focus of several research projects.

In this review, we will delve into a comprehensive discussion of various synthetic strategies employed to conjugate CDs with phthalocyanine (Pc) dyes through covalent and non-covalent interactions to obtain high-performance hybrids. The combination of these two entities has demonstrated remarkable synergistic effects and improved water solubility and biocompatibility with promising outcomes in their applications as nanoprobes for sensing, electrocatalysts, and phototherapeutic agents.[91–95]

2. Functionalization of carbon dots with phthalocyanines

CDs feature various functional groups on their surface, including amino, hydroxyl, and carboxyl units, which enhance their water stability and provide ideal anchoring sites for further functionalization. The chemical versatility of CDs enables them to establish a wide range of interactions with various types of ionic, molecular, and macromolecular entities *via* covalent and non-covalent interactions.[32] Interactions through covalent bonds require the presence of complementary functionalities in the Pcs and CDs. Since CDs can contain abundant carboxyl or amino groups on their surface, coupling mediated by amide bonds must be performed with Pcs bearing amino and carboxyl functionalities, respectively. In general, the esterification approach involves the carboxyl groups of the CDs and hydroxyl groups present on the Pcs, whereas the sulfonylations require CDs functionalized with amino groups and Pcs with sulfonyl chloride functionalities. Most reported covalent strategies are based on amidation and esterification reactions (Fig. 1C). In the development of assemblies of Pc@CDs based on non-covalent bonds, their formation can occur *via* electrostatic, complexation, or π–π interactions (Fig. 1C). These interactions are mainly governed by the inverse surface charges between Pcs and CDs or by the strong quenching promoted by the aromatic nature of Pcs and CDs.

In this review, we delve into a comprehensive discussion of the various strategies employed to covalently and non-covalently conjugate CDs with Pc dyes. The combination of these two entities has demonstrated remarkable synergistic effects, including alterations in fluorescence quantum yield values (φ_f), generation of oxidative species, and improved water solubility and biocompatibility. In recent years, these intriguing Pc@CD nanoconjugates have primarily been applied as nanoprobes for biosensing, electrocatalysts, and antibacterial and phototherapeutic agents.[91,93,96,97] The current section is organized according to the type of interaction involving both components in the hybrid, non-covalent or covalent, which is preceded by a brief reference concerning their impact on the final features of Pc@CDs. In each section, and when possible, the studies are organized based on their application or potential envisaged. Next, we present a detailed discussion of the properties and applications of Pc@CD conjugates based on their non-covalent or covalent nature. Importantly, the inconsistent nomenclature used for CDs in the literature poses a significant challenge in distinguishing between the different types of CDs. To avoid potential misunderstandings, we will use the generic term "CDs" to refer to this class of carbon-based nanomaterials.

2.1. Non-covalent functionalization: electrostatic and/or π–π interaction

2.1.1. Fundamental insights into Pc@CDs' features. The luminescence properties of CDs are extremely dependent on the type of chemical or physical interaction occurring at their surfaces and edges with other molecules that can enhance or quench fluorescence. Since CDs can act as energy donors and electron donors, fluorescence quenching can occur *via* Förster resonance energy transfer (FRET) or by a photo-induced electron transfer (PET) process.[93,98,99] Achadu *et al.* reported, in 2015, a study that can be considered an important basis for further advancements involving Pc@CDs.[100] Based on the electron-donating characteristics of CDs and the behavior of MPcs to act either as electron donors or acceptors, the authors were prompted to evaluate, for the first time, the fluorescence performance of the **ZnPc1@CDs** and **ZnPc2@CDs** conjugates (Fig. 2A) obtained by the adsorption of **ZnPc1** and **ZnPc2** onto CD surfaces through electrostatic and π–π interactions, respect-

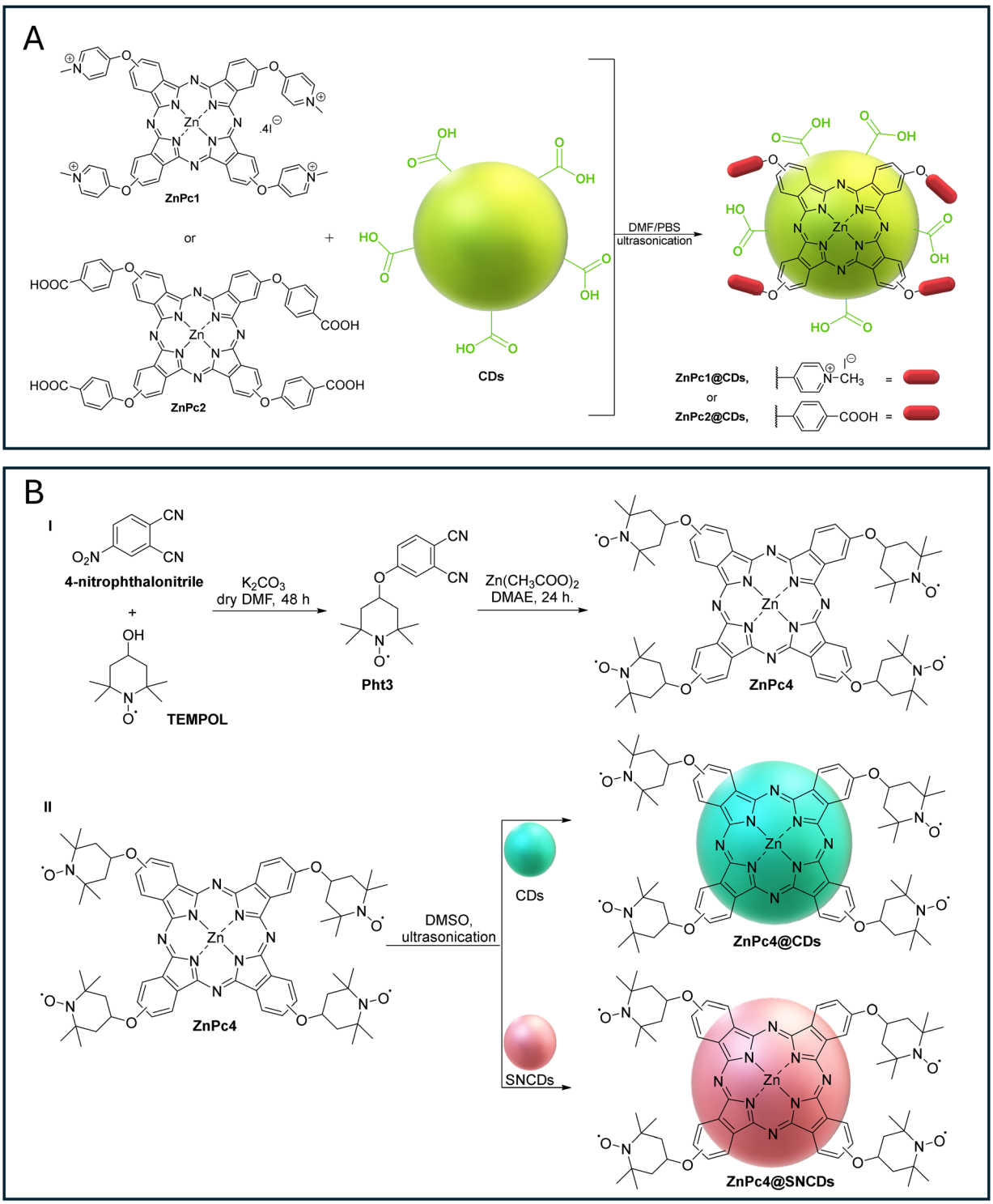

Fig. 2 (A) **ZnPc1@CDs** and **ZnPc2@CDs** obtained *via* ionic and π–π stacking interactions with CDs.[100] (B) (I) Synthesis of **ZnPc4** and hybrids (II) **ZnPc4@CDs** and **ZnPc4@SNCDs**. (III) Graphical representation of selective screening of different biomolecules and metal ions and their effects on the fluorescence response of 0.5 mg mL^{-1} of the **ZnPc4@CD** and **ZnPc4@SNCD** nanoprobes in DMSO.

ively. The CDs were prepared by the oxidation of GO in concentrated H_2SO_4 and HNO_3 under top-down hydrothermal conditions. Zinc(II) phthalocyanines bearing four pyridyloxy substituents (**ZnPc1a**) and four carboxyphenoxy substituents (**ZnPc2**) were obtained by cyclotetramerization of the adequate phthalonitriles (4-(4-pyridyloxy)phthalonitrile (**Pht1**) and 4-(*p*-carboxyphenyloxy)phthalonitrile (**Pht2**), respectively) in pentan-1-ol in the presence of zinc(II) acetate in 1,8-diazabicy-

clo[5.4.0]undec-7-ene (DBU) or DMF.[101,102] Both phthalonitriles (**Pht1** and **Pht2**) were obtained through a nucleophilic *ipso*-nitro substitution reaction involving commercially available 4-nitrophthalonitrile and 4-hydroxypyridine or 4-hydroxybenzoic acid, respectively, in the presence of K_2CO_3. Access to the cationic phthalocyanine **ZnPc1** required an extra step in the quaternization of the pyridyl units of **ZnPc1a** using methyl iodide.

The **ZnPc1@CDs** were obtained by the addition of CDs in phosphate-buffered saline (PBS) solution at pH = 9 to the cationic **ZnPc1** in a DMF/PBS solution, followed by ultrasonication; the alkaline conditions were selected to favor electrostatic interactions between the negatively charged CDs and the positively charged **ZnPc1** (Fig. 2A). The hybrid **ZnPc2@CDs** were obtained under similar conditions, but at pH = 7, to minimize electrostatic repulsion and favor π–π interactions. The extensive evaluation of the photophysical properties of the resulting hybrid materials allowed us to conclude that the fluorescence quenching of the CDs in the hybrids when compared with that of CDs alone (Φ_F = 0.22 *versus ca.* 0.18 for **ZnPc1,2@CDs**) is due to FRET; this conclusion was also supported by an improvement in the emission of the nearby ZnPc acceptors after excitation at 340 nm where the CDs absorb. The low FRET efficiency obtained for both hybrids (**ZnPc1** = 0.18 and **ZnPc2** = 0.14) was justified by the low spectral overlap between the emission of the donors (CDs) and the absorption of the acceptors (ZnPc derivatives). In the same work, the authors found that the covalent attachment of Zn(II) tetraaminophthalocyanine (**ZnTAPc** = **ZnPc3**) to the CDs resulted in a reduction in the fluorescence (Φ_F = 0.12), although the FRET efficiency was higher (Φ_F = 0.45). This behavior was attributed to the closeness of both components and their stronger interactions. Since other mechanisms such as electron transfer or exciton annihilation could also lead to fluorescence quenching, further experimental investigations, such as time-resolved fluorescence spectroscopy or a detailed energy level analysis, would help clarify other contributions to the fluorescence quenching of the CDs in the presence of ZnPcs.

2.1.2. Sensing applications. The possibility of using conjugates based on Pcs and CDs as nanoprobes for different analytes has attracted considerable attention from the scientific community. In this context, the noncovalent assembly of **ZnPc4** bearing (2,2,6,6 tetramethylpiperidin-1-yl)oxyl (**TEMPOL**) units with pristine **CDs** and **CDs** co-doped with S and N (**SNCDs**) was explored to assess their potential as fluorescence nanoprobes for the recognition of ascorbic acid (AA) (Fig. 2B).[103] The selection of TEMPOL was motivated by the high selectivity and specificity of AA for paramagnetic TEMPO derivatives, leading to their conversion into diamagnetic hydroxylamine counterparts. **ZnPc4** was obtained through cyclotetramerization of **Pht3** bearing the radical scavenger TEMPOL unit in DMAE and anhydrous $Zn(CH_3COO)_2$;[104] the **Pht3** was prepared from the condensation of commercially available 4-nitrophthalonitrile with TEMPOL under basic conditions to favor the required nucleophilic *ipso*-nitro substitution reaction. In this work, the authors selected the hydrothermal treatment of citric acid with NaOH at 160 °C to obtain pristine **CDs**, while the **SNCDs** were obtained under the same conditions but NaOH was substituted by thiourea.[105] The noncovalent conjugation *via* π–π stacking interactions of **CDs** and **SNCDs** to **ZnPc4** after ultrasonication in dimethyl sulfoxide (DMSO) was confirmed using Fourier transform infrared (FTIR) spectroscopy, Raman spectroscopy, and ultraviolet-visible (UV-Vis) spectroscopy.[103]

Photophysical studies revealed that the Φ_F and lifetime (τ_f) of CDs decreased significantly upon conjugation with **ZnPc4** (Table 1) due to Förster resonance energy transfer (FRET). The higher FRET efficiency observed for **ZnPc4@SNCDs** (0.92) compared to **ZnPc4@CDs** (0.66) was attributed to a better spectral overlap (*J*). The donor–acceptor distances (8.1 and 9.2 nm) confirmed effective energy transfer within the 1–10 nm range. Titration assays with ascorbic acid (AA) restored the fluorescence of **CDs** and **SNCDs** ("turned ON"), suggesting that AA acted as a spacer or radical scavenger (Fig. 2B). The absence of an enhanced permeation retention (EPR) signal in the paramagnetic nanoassembly further supported this last mechanism. The nanoprobes exhibited high selectivity for AA, with detection limits of 0.2 nM (**ZnPc4@SNCDs**) and 0.8 nM (**ZnPc4@CDs**), and excellent specificity against biomolecules and metal ions (*e.g.*, citric acid, glucose, dopamine, folic acid, Fe^{3+}, or Cl^-) (Fig. 2B). Their application in real sample quantification yielded near-quantitative recoveries, while the spectra of free **CDs** and **SNCDs** remained unchanged in the presence of AA.

The ability of maleimide units to react specifically with thiols *via* Michael addition[110] prompted Achadu *et al.* to develop **ZnPc5@CDs** nanoassemblies (Fig. 3A) to evaluate their potential as nanoprobes of biothiols (*e.g.*, cysteine, homocysteine, or glutathione);[106] these derivatives, which are involved in several biological processes, are increasingly recognized as potential biomarkers for certain diseases. The required **ZnPc5** was synthesized by reacting Zn(II) tetraaminophthalocyanine (**ZnPc3**) with maleic anhydride (Fig. 3A). Pristine CDs were obtained by oxidizing GO in H_2SO_4 and HNO_3. The fluorescence quenching observed in the **ZnPc5@CDs** nanoassemblies was attributed to maleimide attachment. For comparison, maleimide carbon dots (**M@CDs**) were prepared by reacting polyethyleneimine-grafted CDs (**PEI-CDs**) with 4-maleimidobenzoic acid, resulting in a "turn-OFF" state. However, the photoluminescence (PL) intensity of both nanoassemblies was gradually restored upon addition of cysteine, homocysteine, or glutathione but was not affected by the presence of several α-amino acids and proteins. **M@CDs** showed higher sensitivity than **ZnPc5@CDs** due to the direct covalent attachment of maleimide units. No significant fluorescence increase occurred with non-immobilized **ZnPc5** upon adding cysteine, highlighting the key role of CDs in the "turn ON" behavior. However, to complement these studies, a comparison with **ZnPc3**-based nanoassemblies could provide a more realistic idea of the role of maleimide in these hybrids.

Table 1 Summarized properties of **Pc@CD** conjugates for sensing applications

CDs type	Chemical conjugation	Phthalocyanine	$\Phi_{f\ CDs}$	$\Phi_{f\ Pc}$	$\Phi_{f\ hybrid}$	Application	Ref.
SNCDs	Non-covalent (π–π stacking)	2,9(10),16(17),23(24)-Tetrakis[(4-methylpiperidin-1-yl)oxyl]phthalocyaninato zinc(II) (**ZnPc4**)	**SNCDs** (0.81)[a]	*	**ZnPc4@SNCDs** (0.15)[a]	Ascorbic acid detection	103
CDs			**CDs** (0.22)[a]	*	**ZnPc4@CDs** (0.09)[a]		
CDs	Non-covalent (π–π stacking)	2,9(10),16(17),23(24)-Tetrakis(1-pyrrolidine-2,5-dione)phthalocyaninato zinc(II) (**ZnPc5**)	**CDs** (0.31)[b]	**ZnPc5** (0.2)[a]	**ZnPc5@CDs** (0.10)[b]	Biothiol detection (cysteine, homocysteine, or glutathione)	106
PEI-CDs			**PEI-CDs** (0.88)[c]	*	*		
M-CDs			**MCDs** (0.06)[b]	*	*		
PEI-CDs	Non-covalent (π–π stacking)	2,9(10),16(17),23(24)-Tetrakis(2-pyridiniumsulphanyl)phthalocyaninato zinc(II) tetraiodide (**ZnPc6**)	**PEI-CDs** (0.68)[b]	*	**ZnPc6-Au@Ag@PEI-CDs** (0.10)[b]	Biothiol and Hg^{2+} detection	107
PEI-CDs-Au@Ag			**PEI-CDs-Au@Ag** (0.25)[b]				
NCDs	Non-covalent (electrostatic interactions)	2,9(10),16(17),23(24)-Tetrakis(4-pyridiniumsulphanyl)phthalocyaninato zinc(II) tetraiodide (**ZnPc 12**)	**NCDs** (0.10)[d]	**ZnPc12** (0.18)[a]	*	ds-DNA detection	108
		2,3,9,10,16,17,23,24-Octakis(4-pyridiniumsulphanyl) phthalocyaninato zinc(II) octaiodide (**ZnPc 13**)		**ZnPc13** (0.21)[a]			
CDs	Non-covalent (π–π stacking)	2,9(10),16(17),23(24)-Tetrakis(2,6-di-*tert*-butyl-4-methylphenoxy)phthalocyaninato zinc(II) (**CoPc8**)	**CDs** (0.31)[a]	*	*	Cyanide ion detection	109

[a] DMSO. [b] PBS. [c] DMSO : PBS mixture. [d] H_2O.

In the same period, Nyokong *et al.* developed a dual fluorescence nanoprobe, **ZnPc6-Au@Ag@PEI-CDs** (Fig. 3B), for detecting Hg^{2+} and biothiols in aqueous solutions.[107] The sensing platform was assembled by electrostatically combining cationic **ZnPc6** bearing four thiopyridinium units with a nanoalloy **Au@Ag**, followed by embedding the conjugate in **PEI-CDs** obtained from a hydrothermal treatment of GO with hyperbranched polyethyleneimine. The nanoprobe's fluorescence emission was restored in the presence of Hg^{2+} and "turned OFF" upon the addition of biothiols due to their ability to form strong Hg–S bonds (Fig. 3B). These "off–on–off" nanoprobes were stable and selective, with high resistance to interference from other amino acids (glycine, lysine, histidine, tryptophan, or DL-lactic acid) and metal ions (*e.g.*, Fe^{2+}, Co^{2+}, Mn^{2+}, Cd^{2+}, Cu^{2+}, Ni^{2+}, Pb^{2+}, Mg^{2+}, Ag^{+}, and Zn^{2+}). Their effectiveness was confirmed in real samples spiked with test analytes.

A similar concept was considered in the design of "turn-ON" nanoprobes for detecting Hg^{2+}, obtained through the conjugation of CDs with **ZnPc6**, the corresponding Al(III) complex **AlPc6**, **ZnPc7** with eight thiopyridinium moieties, and neutral **ZnPc6a**.[107] The fluorescence of the CDs, derived from GO *via* a hydrothermal method, was initially quenched upon coordination with the Pcs. However, in the presence of Hg^{2+}, the fluorescence was restored due to Hg^{2+}'s strong affinity for mercapto bridges on the Pcs, which disrupted the π–π stacking interaction between the CDs and Pcs. These nanoprobes exhibited high selectivity for Hg^{2+} over other metal ions, with the best limit of detection (LOD) achieved by octacationic **ZnPc7** (0.12 nM), followed by tetracationic **ZnPc6** (LOD = 0.52 nM) and **AlPc6** (LOD = 0.60 nM). The performance was less effective for neutral **ZnPc6a**, confirming the relevance of electrostatic interactions in the development of these nanoassemblies.

Achadu *et al.* described synthetic access to the functional hybrid **CoPc8@CDs** (Fig. 3C) and demonstrated its use as a selective "turn ON" nanoprobe for CN^{-}.[111] The CDs were synthesized by a top-down hydrothermal process, and the Schiff complex **CoPc8** was obtained by coupling tetraamino cobalt(II) phthalocyanine **CoPc3** with 1-pyrene-1-carboxyaldehyde. The nanoassemblies obtained upon its conjugation with the CDs showed a typical "turn-OFF" behaviour.

The sensing studies showed that in the presence of the anion cyanide, the CDs' emission was restored and increased linearly with the concentration of CN^{-} (ranging between 1 nM and 50 nM) with a LOD of 0.5 nM. The probe's selectivity for CN^{-} was confirmed through fluorescence recovery assessments in water samples containing various anions (*e.g.*, F^{-}, Cl^{-}, Br^{-}, I^{-}, $H_2PO_4^{-}$, HSO_4^{-}, NO_3^{-}, ClO_4^{-}, SCN^{-}, AcO^{-}, HSO_3^{-}, SO_4^{2-}, and CO_3^{2-}). The inefficacy of the analogous **ZnPc8** complex in anion detection supports the hypothesis that axial coordination between the Co metal ion in the Pc inner core and CN^{-} is responsible for disrupting the initial donor–acceptor "turn-OFF" behavior. Considering this fact, to evaluate the real role of the pyrene units in Pc, it would be interesting to compare the sensing results obtained with the nanoassemblies

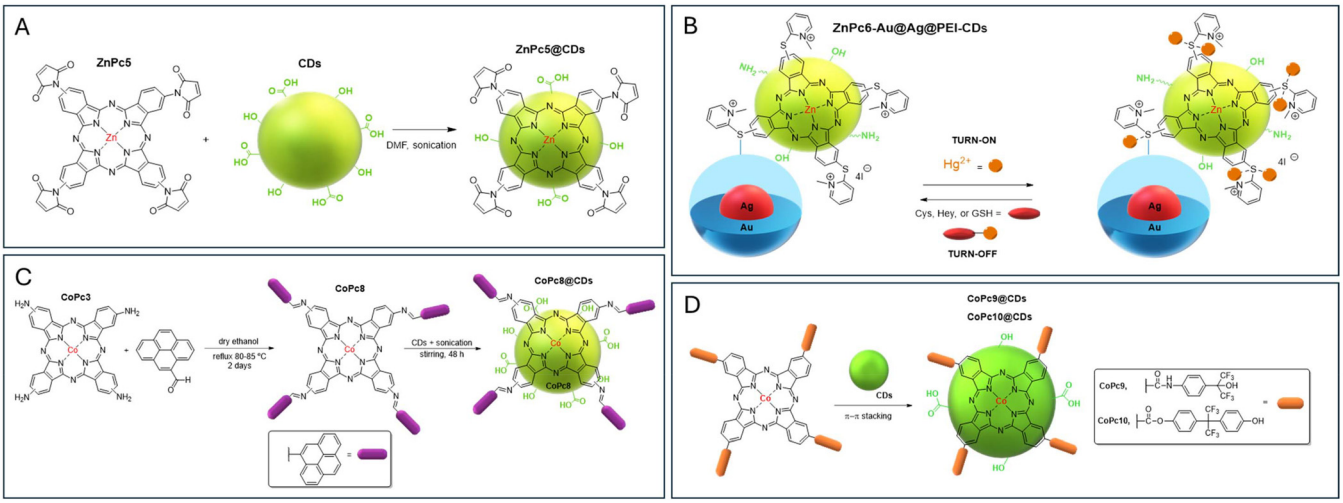

Fig. 3 (A) Representation of the **ZnPc5@CD** nanoassemblies.[106] (B) Proposed mechanistic actuation of the "off–on–off" nanoprobe **ZnPc6-Au@Ag@PEI-CDs** for the detection of Hg^{2+} and biothiols in aqueous solutions.[107] (C) Synthetic route for pyrene-derivatized **CoPc8** and **CoPc8@CD** hybrids.[111] (D) Structures of **CoPc9** and **CoPc10** used for the preparation of **CoPc9,10@CD** hybrids.[112,113]

obtained from tetraamino cobalt(II) phthalocyanine **CoPc3** or even with non-substituted **CoPc**. The efficiency of this probe in evaluating trace levels of CN^- ions in a real context was confirmed using tap water spiked with known concentrations of CN^- between 0.5 and 50 nM with percentage recoveries higher than 97%.

The efficiency of Pc@CD hybrids for gas detection, namely at room temperature, is also attracting some attention. In 2021, Jiang *et al.* developed nanoassemblies from CDs and CoPc dyes containing hexafluoroisopropanol (HFIP, **CoPc9**) and hexafluorobisphenol A (6FBPA, **CoPc10**) substituents (Fig. 3D) and explored their efficiency as sensors towards the chemical warfare agent simulant dimethyl methylphosphonate (DMMP).[112] The **CoPc9,10@CD** hybrids showed strong hydrogen bonds between the two functional units (HFIP and 6FBPA) and the DMMP molecule, leading to an exceptional response behaviour to the analyte. Moreover, it has been reported that the CDs improved the electrical conductivity of the hybrids by π–π interactions with CoPcs and can be considered promising raw materials for use in sarin gas sensors.

In 2021, Zhi Yang *et al.* developed hybrid materials for NO_2 gas sensing based on the anchorage of CDs onto the surface of **MPc11** (where Pc is 2,9,16,23-tetracarboxylicphthalocyanine and M = Co, Ni, Cu, or Zn) nanofibers *via* π–π stacking interactions to form a charge transfer conjugate.[113] The addition of CDs greatly increased the conductivity of the Pc fibers, leading to a faster response of the hybrid materials up to 14.5 nA. The sensing mechanism is based on the typical p-type semiconductor behaviour of **MPc11@CDs**, which have a strong affinity for the electron acceptor molecule NO_2. Consequently, after the reaction with the complex, the electrons are trapped by NO_2, producing NO_2^- ions and holes on the nanofiber surface, significantly changing the conductivity of the sensors. The gas-sensitive response (*I–V* curves) of the **CoPc@CD** hybrid material to 50 ppm NO_2 gas was nearly 16 times higher compared with the individual components. Moreover, the reproducibility, selectivity, and stability of the hybrids are significantly enhanced. The response value was achieved within 100 s, and the recovery curve reached the baseline 125 s after laser exposure.

In the context of biosensing applications, Santiago *et al.* reported in 2022 that the **ZnPc12@NCD** and **ZnPc13@NCD** nanoprobes (Fig. 4A) can induce an "off–on" fluorescence behaviour on nitrogen doped carbon dots (NCDs) after interacting with double-stranded DNA (ds-DNA). These nanoprobes were obtained from positively charged **ZnPc12** and **ZnPc13** and NCDs prepared by the hydrothermal treatment of GO in the presence of NH_4OH and H_2O_2.[108] The ZnPcs were synthesized using the conventional tetramerization of suitable phthalonitriles bearing one or two thiopyridyl units in DMAE and in the presence of $Zn(OAc)_2$, followed by quaternization of the pyridine units with CH_3I. Supramolecular **Pc@NCD** hybrids were prepared in water using solutions of NCDs and Pcs in a molar ratio of 1 : 5. This conjugation promoted quenching of the emission of NCDs, but in the presence of ds-DNA, their photoluminescence was restored. This behaviour was justified by the preferential interaction between the positively charged Pcs and the negatively charged dsDNA, with the consequent restoration of the NCDs' photoluminescence. The limits of detection obtained for ds-DNA with **ZnPc13** and **ZnPc12** were 66 nM bp and 1.1 mM bp (bp = molar concentration of pairs), respectively. The concentration difference used for each Pc dye is most likely associated with their solubility, depending on the number of peripheral substituents (four *versus* eight). Both nanosensors exhibit good selectivity for ds-DNA when tested against biothiols and inorganic anions as potential interferents (Fig. 4B).

2.1.3. Photosensitizing applications. Molecules, commonly known as PSs, that generate reactive oxygen species (ROS) upon excitation with visible light are particularly relevant in

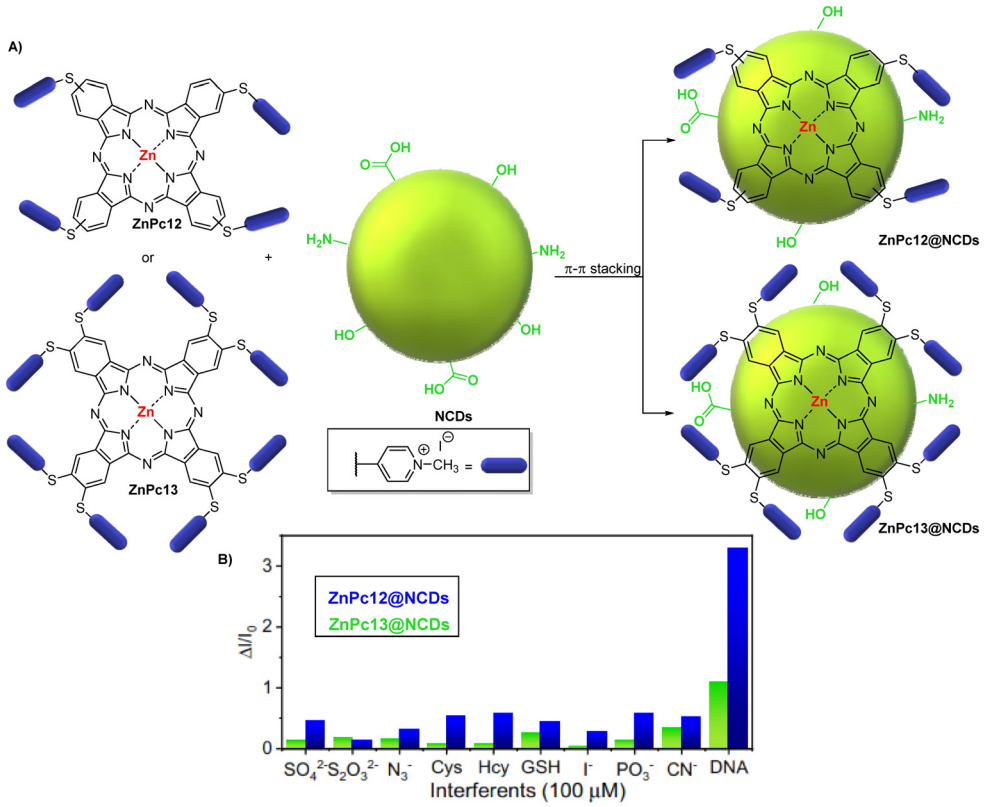

Fig. 4 (A) Structures of **ZnPc12,13** used in the formation of **ZnPc12,13@NCD** nanohybrids. (B) Selectivity of the nanosensors (**ZnPc12@NCDs** and **ZnPc13@NCDs** with a 1 : 5 ratio of Pc : NCDs and [NCDs] = 2 μM) towards ds-DNA, showing photoluminescence enhancement in the presence of an excess (100 μM) of various relevant analytes. Reproduced under terms of the CC BY 4.0 license.[108] Copyright 2022, MDPI.

various applications, including PDT, aPDT, and photocatalysis. Pc-based compounds, in particular, are recognized as promising candidates owing to their high efficiency in generating ROS, namely $^1O_2$ species.

Despite these advantageous properties, the low solubility of Pcs in aqueous media and their lack of specificity pose significant challenges for their biological applications. To overcome these limitations, researchers have investigated the conjugation of Pcs with carbon-based nanomaterials. Among these, CDs have emerged as an appealing choice because of their high biocompatibility, water solubility, and efficient cellular internalization.[114,115] The following sections discuss various approaches reported in the literature for synthesizing Pc-based CDs and assessing their performance in terms of emission quantum yield and ROS generation. Such insights are crucial for advancing solutions involving PSs, particularly Pcs. These applications include tumour cell eradication, microorganism inactivation and photocatalysis, underscoring the diverse potential of Pc@CDs in photosensitizing processes.

2.1.3.1. Cancer therapy. To identify efficient Pc@CD hybrids for phototherapeutic applications, Matshitse *et al.* evaluated how the physicochemical features of the obtained nanoassemblies through electrostatic and/or π–π interactions were affected by the Pc charge. This systematic study was performed using unsubstituted **ZnPc**, **ZnPc1** bearing *N*-methylpyridyloxy units, and tetrasulfonated **ZnPc14** as prototypes, respectively, of neutral, positively, and negatively charged derivatives to construct the corresponding CD nanoassemblies (Fig. 5A).[116] CDs with a size near 2.2 nm were obtained through the chemical oxidation of GO using $KMnO_4$ and H_2SO_4 as oxidative agents.[117] The successful conjugation was confirmed by different characterization techniques, and it was concluded that the largest loading was observed for **ZnPc1@CDs** (14 Pc molecules per CD *versus* 4 for **ZnPc** and 3 for **ZnPc14**). These results were attributed to the establishment of both π–π and electrostatic interactions between the negatively charged CDs and the positively charged **ZnPc1**.

The results showed that the Φ_F of CDs in DMSO decreased from 11% to 2% upon conjugation to **ZnPc1** and **ZnPc** and to ~8% for **ZnPc14**. This quenching was accompanied by a decrease in τ_f. The lower quenching observed for **ZnPc14@CDs** was attributed to its lower loading, which reduces aggregation. FRET efficiency analysis indicated a strong energy transfer for **ZnPc@CDs** (0.81) and **ZnPc1@CDs** (0.80), while **ZnPc14@CDs** had a lower efficiency (0.28) due to electrostatic repulsion increasing the donor–acceptor distance (Table 2). **ZnPc1@CDs** showed the highest FRET efficiency due to the attractive interactions between oppositely charged surfaces. Despite increased triplet quantum yields (Φ_T) upon conjugation, this increase was not reflected in the Φ_Δ values of the hybrids that

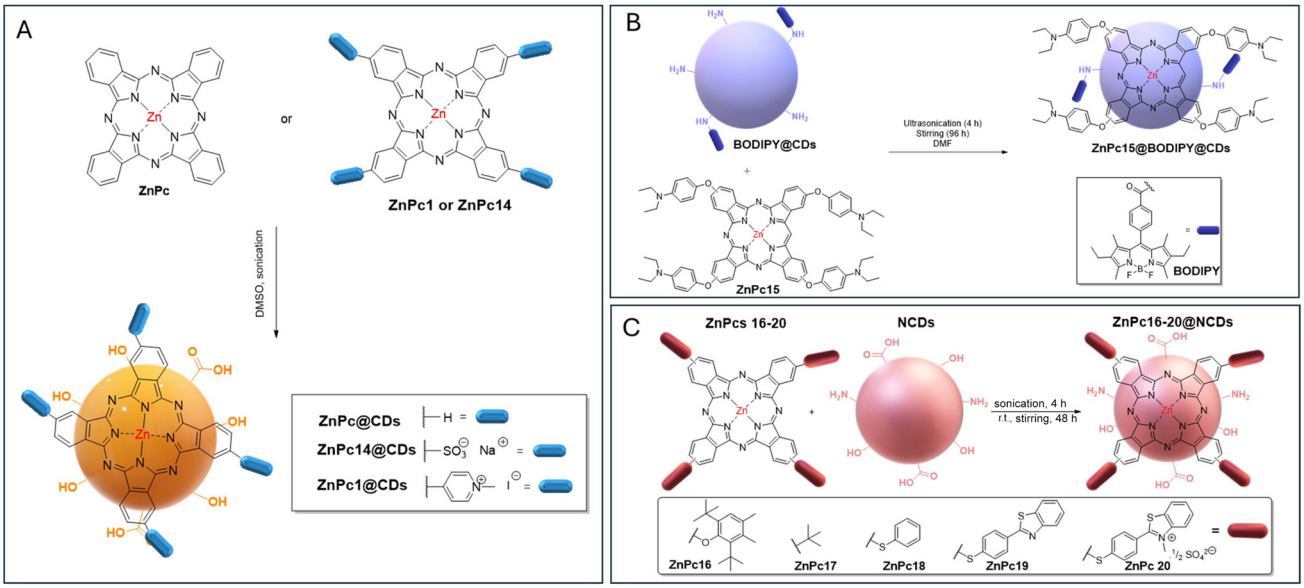

Fig. 5 (A) The structures of neutral, negatively charged, and positively charged Pc dyes used to evaluate the impact of charge type on the physicochemical features of ZnPc@CDs.[116] (B) Formation of **ZnPc15@BODIPY@NCD** conjugates *via* covalent conjugation of NCDs with BODIPY and subsequent π–π interactions with **ZnPc15**.[118] (C) Structures of **ZnPc16–20** for the preparation of **ZnPc16–20@NCDs** *via* π–π interactions.[119]

remained lower than that of ZnPc alone (Φ_Δ = 0.67) or similar to those of free **ZnPc1** (Φ_Δ = 0.41) and **ZnPc14** (Φ_Δ = 0.32). This fact was attributed to a screening effect that prevented efficient energy transfer to the ground state of molecular oxygen. Additionally, the presence of water further quenched $^1O_2$, contributing to their lower Φ_Δ values, when measured in this solvent.[110]

To evaluate how the size of CDs could affect the ability of Pcs to generate $^1O_2$, Matshitse *et al.* considered the development and photophysical/photochemical characterization of assemblies based on cationic **ZnPc1** and CDs of different sizes denoted as CD_2 (2.6 nm), CD_6 (3.3 nm), and CD_{10} (5.1 nm).[125] These CDs were prepared *via* the chemical cutting of GO using $KMnO_4$ and H_2SO_4 as oxidative agents and varying the reaction time from 2 to 6 h.[117] The results showed that the atomic concentrations of oxygen decreased with increasing sizes of CDs leading to a blue shift in their spectra and can justify the lower Pc loading found for this assembly (3 *versus* 10 for **ZnPc1@CDs$_{10}$** and **ZnPc1@CDs$_2$** and 5 for **ZnPc1@CD$_6$**). Compared with the initial **ZnPc1** (Φ_Δ = 0.03), the presence of CDs improved the Φ_Δ values in water, with the best performance observed for **ZnPc1@CD$_6$** (Φ_Δ = 0.27), followed by **ZnPc1@CD$_2$** (Φ_Δ = 0.17) and **ZnPc1@CD$_{10}$** (Φ_Δ = 0.11). The low performance of **ZnPc1@CD$_2$** with the highest number of Pcs was attributed to the aggregation effects. This study showed that the structural features of CDs, namely, size, the amount of oxygen, and the presence of Pc, can have an important impact on their phototherapeutic or photocatalytic applications.

In 2018, Nyokong *et al.* reported the synthesis of supramolecular hybrids constituted of **ZnPc15** bearing diethylaminophenoxy substituents embedded in nitrogen CDs covalently linked through an amide bond to carboxylic acid bordipyrromethane (**BODIPY@NCDs**) (Fig. 5B).[118] The photophysical characterization of the **ZnPc15@BODIPY@NCDs** hybrids showed a slight decrease in both the Φ_F and τ_F values when compared with the CDs alone (0.23 and 2.84 ns *versus* 0.27 and 3.41 ns). The decrease in Φ_F values could be due to the FRET behaviour. Regarding $^1O_2$ production, **ZnPc15@BODIPY@NCDs** (Φ_Δ = 0.70) displayed an improved $^1O_2$ generation ability compared to **ZnPc15** (Φ_Δ = 0.50) in DMSO.

In 2019, Nene *et al.* evaluated for the first time the phototherapeutic efficiency of conjugates obtained from a series of ZnPcs (**ZnPc16–20**) with CDs in human breast cancer MCF-7 cell lines (Fig. 5C).[119] The nitrogen-doped CDs used in the synthesis of **ZnPc16–20@NCDs** assemblies were obtained from GO and ammonia. The results showed that the photophysical/photochemical features of ZnPcs were affected upon conjugation with CDs by π–π interactions, showing a decrease in the Φ_F value of the Pcs, which was accompanied by an increase in the Φ_T value. All conjugates were able to generate $^1O_2$ species, although with slightly less efficiency than the non-conjugated **ZnPc**, probably because the CDs' screening effect limits the facile energy transfer from the triplet state to dioxygen. The **ZnPc@NCDs** conjugates demonstrated PDT activity in the human breast cancer MCF-7 cell line upon irradiation, with the best results obtained for the **ZnPc19@NCDs** and **ZnPc20@NCDs** conjugates when compared with the corresponding non-immobilized **ZnPc**. At the highest conjugate concentration (100 μg mL^{-1}), cytotoxicity was approximately 50%.

Soon after, the authors reported the development and photodynamic efficiency towards MCF-7 cell lines of the novel hybrid materials **ZnPc21,22@NCDs** and **ZnPc21,22@biotin-NCDs** containing neutral and cationic morpholine-substituted

Table 2 Summary of the properties of non-covalently bonded **Pc@CD** conjugates for cancer therapy and bioimaging

CDs type	Chemical conjugation	Phthalocyanine	Φ_{CD}	Φ_{Pc}	Φ_{hybrid}	Application	Ref.
CDs	Non-covalent (π–π stacking)	Zinc(II) phthalocyanine (**ZnPc**)	**CDs** (0.11)[a]	*	**ZnPc@CDs** (0.021)[a]	Determination of Φ_{Δ} values	119
		2,9(10),16(17),23(24)-Tetrakis[4-(*N*-methylpyridyloxy)]phthalocyaninato zinc (II) (**ZnPc1**)		*	**ZnPc1@CDs** (0.022)[a]		
		2,9(10),16(17),23(24)-Tetrakis(4-sulfonatophenyl)phthalocyaninato zinc(II) (**ZnPc14**)		*	**ZnPc14@CDs** (0.079)[a]		
NCDs	Non-covalent (π–π stacking)	2,9(10),16(17),23(24)-Tetrakis(2,6-di-*tert*-butyl-4-methylphenoxy)phthalocyaninato zinc(II) (**ZnPc16**)	**NCDs** (0.17)[a]	**ZnPc16** (0.16)[a] **ZnPc16** (0.78)[b] **ZnPc16** (0.50)[c]	**ZnPc16@NCDs** (0.09)[a] **ZnPc16@NCDs** (0.77)[b] **ZnPc16@NCDs** (0.30)[c]	PDT against MCF7 breast cancer cells	119
NCDs	Non-covalent (π–π stacking)	2,9(10),16(17),23(24)-Tetrakis(*tert*-butyl) phthalocyaninato zinc(II) (**ZnPc17**)	**NCDs** (0.17)[a]	**ZnPc17** (0.18)[a] **ZnPc17** (0.77)[b] **ZnPc17** (0.49)[c]	**ZnPc17@NCDs** (0.17)[a] **ZnPc17@NCDs** (0.83)[b] **ZnPc17@NCDs** (0.40)[c]	PDT against MCF7 breast cancer cells	119
NCDs	Non-covalent (π–π stacking)	2,9(10),16(17),23(24)-Tetrakis (phenylsulphanyl)phthalocyaninato zinc (II) (**ZnPc18**)	**NCDs** (0.17)[a]	**ZnPc18** (0.14)[a] **ZnPc18** (0.65)[b] **ZnPc18** (0.50)[c]	**ZnPc18@NCDs** (0.01)[a] **ZnPc18@NCDs** (0.67)[b] **ZnPc18@NCDs** (0.45)[c]	PDT against MCF7 breast cancer cells	119
NCDs	Non-covalent (π–π stacking)	2,9(10),16(17),23(24)-Tetrakis[(thiophenyl) benzo[*d*]thiazole]phthalocyaninato zinc(II) (**ZnPc19**)	**NCDs** (0.17)[a]	**ZnPc19** (0.18)[a] **ZnPc19** (0.67)[b] **ZnPc19** (0.54)[c]	**ZnPc19@NCDs** (0.11)[a] **ZnPc19@NCDs** (0.70)[b] **ZnPc19@NCDs** (0.50)[c]	PDT against MCF7 breast cancer cells	119
NCDs	Non-covalent (π–π stacking)	2,9(10),16(17),23(24)-Tetrakis[(thiophenyl) benzo[*d*]thiazolium]phthalocyaninato zinc (II) sulfate (**ZnPc20**)	**NCDs** (0.17)[a]	**ZnPc20** (0.10)[a] **ZnPc20** (0.75)[b] **ZnPc20** (0.35)[c]	**ZnPc20@NCDs** (0.09)[a] **ZnPc20@NCDs** (0.77)[b] **ZnPc20@NCDs** (0.30)[c]	PDT against MCF7 breast cancer cells	119
NCDs-biotin	Non-covalent (π–π stacking)	2,9(10),16(17),23(24)-Tetrakis[2,5-dimethyl-4-(methylmorpholino)-phenoxy] phthalocyaninato zinc(II) (**ZnPc21**)	**NCDs-biotin** (0.24)[a]	**ZnPc21** (0.20)[a] **ZnPc21** (0.68)[b]	**ZnPc21@NCDs-biotin** (0.16)[a] **ZnPc21@NCDs-biotin** (0.72)[b]	PDT against MCF7 breast cancer cells	120
			NCDs-biotin (0.25)[d]	**ZnPc21** (0.67)[c]	**ZnPc21@NCDsbiotin** (0.47)[c]		
NCDs	Non-covalent (π–π stacking)	2,9(10),16(17),23(24)-Tetrakis[2,5-dimethyl-4-(methylmorpholin-4-ium)phenoxy] phthalocyaninato zinc(II) disulfate (**ZnPc22**)	**NCDs** (0.17)[a]	**ZnPc22** (0.20)[a] **ZnPc22** (0.69)[b] **ZnPc22** (0.53)[c]	**ZnPc22@NCDs** (0.15)[a] **ZnPc22@NCDs** (0.74)[b] **ZnPc22@NCDs** (0.58)[c]	PDT against MCF7 breast cancer cells	120
			NCDs (0.20)[d]	**ZnPc22** (0.14)[d] **ZnPc22** (0.11)[e]	**ZnPc22@NCDs** (0.10)[d] **ZnPc22@NCDs** (0.08)[e]		
NCDs-biotin	Non-covalent (π–π stacking)	2,9(10),16(17),23(24)-Tetrakis[2,5-dimethyl-4-(methylmorpholin-4-ium)-phenoxy] phthalocyaninato zinc(II) disulfate (**ZnPc22**)	**NCDs-biotin** (0.24)[a]	**ZnPc22** (0.20)[a] **ZnPc22** (0.69)[b] **ZnPc22** (0.53)[c]	**ZnPc22@NCDs-biotin** (0.14)[a]	PDT against MCF7 breast cancer cells	120
			NCDs-biotin (0.25)[d]	**ZnPc22** (0.14)[d] **ZnPc22** (0.11)[e]			
NCDs	Non-covalent (π–π stacking)	2,9(10),16(17),23(24)-Tetrakis(*N*-methyl-morpholin-4-ium)phthalocyaninato zinc(II) disulfate (**ZnPc23**)	**NCDs** (0.70)[a]	**ZnPc23** (0.16)[a]	**ZnPc23@NCDs** (0.14)[a]	PSDT against MCF-7 breast cancer cells	121
SNCDs	Non-covalent (electrostatic interactions)		**SNCDs** (0.80)[a]	**ZnPc23** (0.16)[a]	**ZnPc23@SNCDs** (0.14)[a]		
GQDs@cysteine	Non-covalent (electrostatic interactions	4-Tetra-(2-bromo-4-methylphenol) phthalocyaninato indium(III) chloride	**GQDs@cysteine** (0.41)[a]	**InPcBr** (0.02)[a] (0.75)[c] (0.96)[f]	**InPcBr@ GQDs@cysteine** (0.81)[c] (1.31)[f]	Determination of Φ_{Δ} values using sono-photochemical methodologies	122

Table 2 *(Contd.)*

CDs type	Chemical conjugation	Phthalocyanine	Φ_{CD}	Φ_{Pc}	Φ_{hybrid}	Application	Ref.
GQDs@cysteine	Non-covalent (electrostatic interactions)	Tetrakis(2-bromo-4-methylphenoxy) phthalocyaninato zinc(II)	**GQDs@cysteine** (0.41)[a]	**ZnPcBr** (0.20)[a] (0.63)[c] (0.94)[f]	**ZnPcBr@GQDs@cysteine** (0.68)[c] (0.95)[f]	Evaluation of the photochemical properties using sono-photodynamic procedures	123
		Tetrakis(2-chloro-4-methylphenoxy) phthalocyaninato zinc(II)		**ZnPcCl** [0.24][a] (0.55)[c] (0.91)[f]	**ZnPcCl@GQDs@cysteine** (0.57)[c] (0.93)[f]		
GQDs@cysteine	Non-covalent (electrostatic interactions)	4-Tetrakis(2-chloro-4-methylphenoxy) phthalocyaninato indium(III) chloride	**GQDs@cysteine** (0.41)[a]	**InPcCl** (0.02)[a] (0.65)[c] (0.94)[f]	**InPcCl@GQDs@cysteine** (0.79)[c] (1.17)[f]	Assessment of singlet oxygen yield, Φ_Δ, using ultrasound and light	124

[a] Φ_f in DMSO. [b] Φ_T in DMSO. [c] Φ_Δ in DMSO. [d] Φ_f in H_2O. [e] Φ_Δ in H_2O. [f] Φ_Δ in DMSO using ultrasound at 35 kHz and light exposure at 7.05×10^{15} photons s^{-1} cm^{-2}.

Pcs **ZnPc21** and **ZnPc22** and NCDs without or with tumour-targeting biomolecules such as biotin (Fig. 6).[120] Access to neutral **ZnPc21** and cationic **ZnPc22** required the synthesis of the precursor 4-(2,5-dimethyl-4-(morpholinomethyl)phenoxy) phthalonitrile (**Pht4**) by the reaction of 2,5-dimethyl-4-(morpholinomethyl)-phenol hydrochloride monohydrate with commercially available 4-nitrophthalonitrile followed by their tetramerization in the presence of $Zn(OAc)_2$, affording **ZnPc21**. The cationic **ZnPc22** was obtained by quaternization of the morpholino units in the presence of dimethylsulfate (DMS) or DMF (Fig. 6A). NCDs functionalized with biotin were prepared by reacting NCDs with biotin in the presence of the carboxyl-activating reagents *N*,*N*′-dicyclohexylcarbodiimide (DCC) and 4-dimethylaminopyridine (DMAP) in DMF.[120] The synthesis of the nanoplatforms required sonication followed by stirring (Fig. 6B).

The photophysical characterization of the **ZnPc21,22@NCD** and **ZnPc21,22@biotin-NCD** nanoassemblies showed that the conjugation caused quenching of the emission and also a drop in the Φ_Δ values owing to screening effects. However, an increase in PDT activity was observed for the cationic dye in combination with biotin-functionalized NCDs. The PDT activity of the complexes (less cell viability) of **ZnPc21** and **ZnPc22** was higher than that of their non-functionalized CD conjugates. For **ZnPc21@CDs**, the low PDT activity may be related to its low Φ_Δ values when compared to the non-immobilized **ZnPc21** (Table 2). Indeed, cationic complexes generally perform better than non-charged complexes. This has previously been reported for Pcs[126] and other charged complexes in cancers,[127,128] where the net anionic membrane charge of cancer cells is believed to be susceptible to cationic drug complexes through electrostatic attraction. This may result in improved drug retention, and hence, more available Pcs for therapy. The combination of charge and biotin ligands improved the therapeutic efficacy of the complex.

In a related study, Nyokong *et al.*[121] reported the preparation of **ZnPc23@NCD** and **ZnPc23@NSCD** nanoassemblies by conjugating cationic **ZnPc23** bearing morpholino moieties with **NCDs** and **NSCDs** (Fig. 7A). The **NCDs** and **NSCDs** were synthesized from citric acid under hydrothermal conditions (180 °C, 5 h) using urea and thiourea, respectively. The efficiency of the obtained assemblies was evaluated for the treatment of MCF7-cells under PDT, sonodynamic therapy (SDT), and combined PDT plus SDT (PSDT). Pc, CDs, and hybrids demonstrated cytotoxicity for PDT, SDT, and PSDT treatments in a concentration-dependent manner due to cellular oxidative stress generated by the formation of ROS (Fig. 7B). The determined IC_{50} values showed that Pc presented a relatively lower value than the conjugates for all three explored therapies. The results showed that $^1O_2$ was generated under all therapeutic conditions and its presence increased upon conjugation. However, the generation of $^{\bullet}OH$ radicals, which played a significant role in the eradication of cancer cells, only generated in the SDT and PSDT assays, showing a decrease in signal intensity after the conjugation of Pc to the CDs (Table 2).

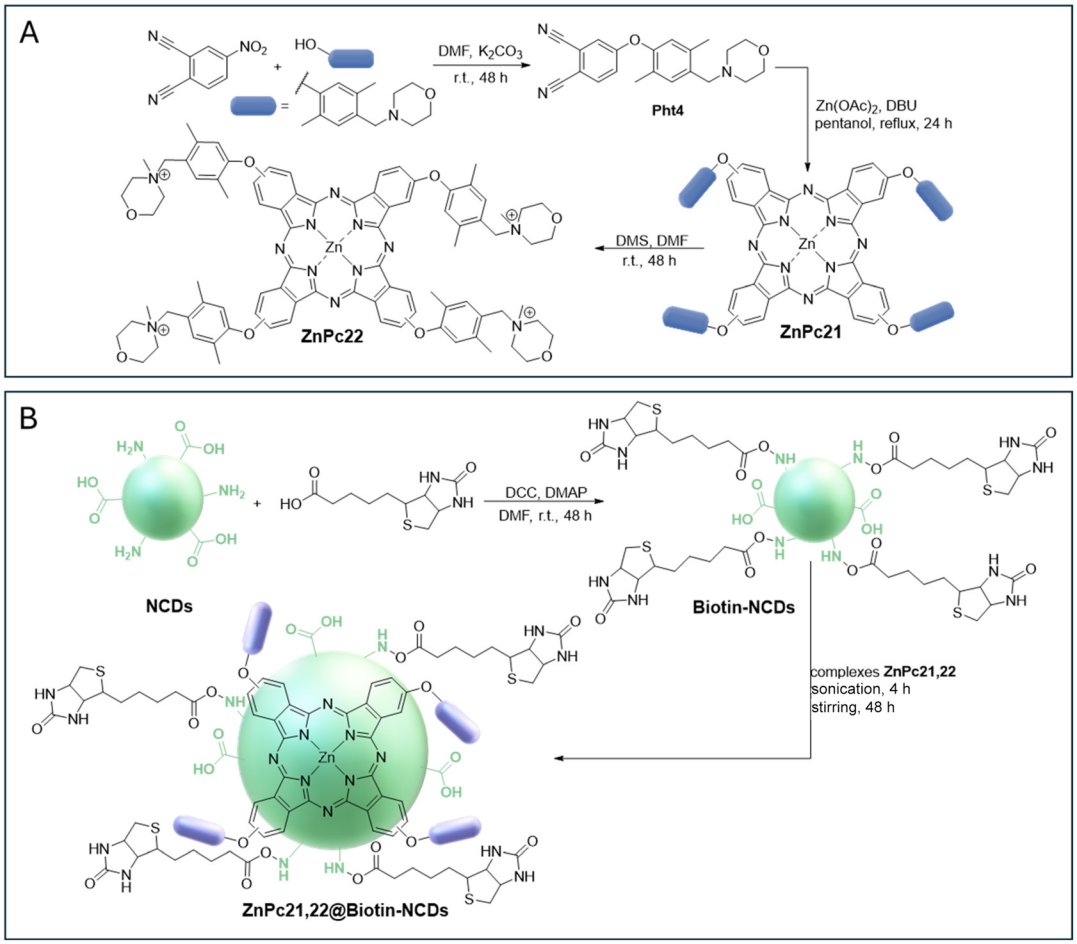

Fig. 6 (A) Synthesis of **ZnPc21** and **ZnPc22**. (B) Synthesis of **biotin-NCDs** and **ZnPc21, 22@biotin-NCD** conjugates.[120]

Knowing that current PDT agents often suffer from low singlet oxygen quantum yields, photobleaching, and poor biocompatibility, Erdoğmus *et al.*[122–124] developed new hybrid nanomaterials to address these issues, based on the conjugation of indium(III) and zinc(II) phthalocyanines with halogen and phenoxy substituents using GQDs obtained from citric acid and cysteine (GQDs@cysteine) under hydrothermal conditions. Specifically, tetrakis(2-bromo-4-methylphenoxy)phthalocyaninato zinc(II), tetrakis(2-chloro-4-methylphenoxy)phthalocyaninato zinc(II), 4-tetrakis(2-chloro-4-methylphenoxy) phthalocyaninato indium(III) chloride, and 4-tetrakis(2-bromo-4-methylphenoxy)phthalocyaninato indium(III) chloride as regioisomeric mixtures were immobilized onto GQDs@cysteine through π–π stacking interactions. The photochemical and sonophotochemical properties of the resulting nanomaterials and their precursors were evaluated for potential applications in advanced cancer treatments with enhanced $^1O_2$. Briefly, all derivatives were exposed to light, sound, or a combination of both to measure their singlet oxygen production yield. The nanoconjugates of InPc and ZnPc exhibited improved Φ_Δ, compared to non-conjugated Pcs. In addition, it was observed that indium, being heavier than zinc, enhanced intersystem crossing and gave a higher singlet oxygen production yield (Table 2). These three studies confirmed that the sono-photodynamic approach (SPDT) enhances therapeutic efficacy by combining the advantages of light and ultrasound.

2.1.3.2. Antibacterial applications. The conjugation of the CDs and Pcs was also explored for antibacterial applications (Table 3), considering previous reports that showed improvements in the required photophysicochemical features after the formation of the hybrids. Nyokong *et al.* conducted the first study in the context of aPDT using **MPc24@CD** nanoassemblies (M = 2H, Zn, or In) against the multidrug-resistant *Staphylococcus* (Fig. 8).[129] The photoactive platforms were prepared from the free-base **H_2Pc24** with acetylphenoxy units and the corresponding **ZnPc24** and **InPc24** complexes (Fig. 8A). In the selection of these Pcs, the authors took into account the antibacterial features associated with the reactive carbonyl group.[130,131] The synthetic strategy involved the reaction of 4-hydroxyacetophenone with 4-nitrophthalonitrile to afford the required phthalonitrile **Pht5**, followed by its tetramerization in DMAE and DBU with LiCl or $ZnCl_2$ to obtain **H_2Pc24** or **ZnPc24**, respectively (Fig. 8A).[129] **InPc14** was obtained by the reaction of **H_2Pc24** with anhydrous InCl in dry DMF and DBU.

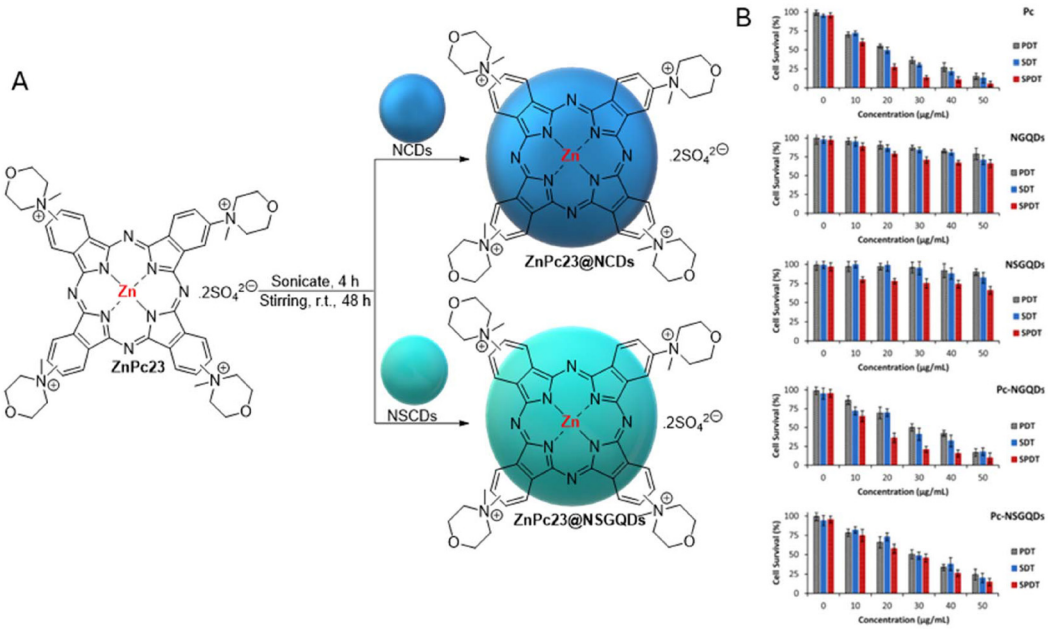

Fig. 7 (A) Structures of **ZnPc23@NCD** and **ZnPc23@NSCD** conjugates. (B) WST-assay post-PDT, SDT, and PSDT treatments at varied concentrations in water at 10 min irradiation time, n = 3. Parameters: PDT = irradiation dose of 170 J cm^{-2}, power 2.3 W at 680 nm. SDT: frequency = 1 MHz, power = 1 W cm^{-2}, 100% duty cycles. PSDT = combined PDT and SDT parameters with PDT applied first. Reproduced with permission.[121] Copyright 2021, Elsevier B.V.

The results showed that the efficiency of the conjugates at producing $^1O_2$ parallels that observed by the non-conjugated Pcs, with the indium complex being the most efficient, followed by the zinc complex, and then the free base (values ranging from Φ_Δ = 0.20 to 0.79 in DMSO). The aPDT activity of both phthalocyanines and nanoconjugates was tested against multidrug-resistant *Staphylococcus aureus* (*S. aureus*), where **InPc24@CDs** were highly effective causing a 9.68 log reduction in the bacterial viability at 10 μM (based on Pc) when compared to the 3.77 log reduction of **ZnPc24@CDs** (Fig. 8C and D).

The photodynamic action of **ZnPc25@NCD** nanoassemblies, obtained from nitrogen-doped CDs (**NCDs**) and **ZnPc25** bearing benzoimidazolylphenoxy units, was evaluated towards Gram-positive bacteria *S. aureus*.[132] The hybrid constituents were obtained following well-established approaches, and the photophysical/photochemical characterization showed improved singlet oxygen (Φ_Δ = 0.45) and triplet state quantum yields (Φ_T = 0.60) compared to the non-immobilized **ZnPc25** (Φ_Δ = 0.36 and Φ_T = 0.54). In the antibacterial tests under UV light exposure, the **ZnPc25@NCD** hybrid achieved a 99.9% bacterial kill rate, outperforming free **ZnPc25** (99.86%). This aligns with its higher singlet oxygen production. In 2024, Özçesmeci *et al.* reported the synthesis of new nanoconjugates through the non-covalent conjugation of copper(II) phthalocyanine, substituted with 2,3-dihydroxypropoxy groups in the non-peripheral positions, with carbon dots (**CDs**) and carbon-boron quantum dots (**CBDs**). The antimicrobial photodynamic therapy (aPDT) efficacy of each hybrid was evaluated against Gram-positive bacteria (*E. hirae* and *E. faecalis*), Gram-negative bacteria (*E. coli*, *P. aeruginosa*, and *B. subtilis*), and microfungi (*C. parapsilosis* and *C. albicans*). The selected phthalocyanine was obtained by deprotecting the (2,2-dimethyl-1,3-dioxolan-4-yl)methoxy groups in 1,8(11),15(18),22(25)-tetrakis[(2,2-dimethyl-1,3-dioxolan-4-yl)methoxy]phthalocyaninato copper (II) using acetic acid. The **CBDs** were synthesized *via* microwave-assisted synthesis, involving citric and boric acids. The aPDT evaluation revealed the lowest minimum inhibitory concentration (MIC) of 4 mg L^{-1} against Gram-positive bacteria, which decreased further post-irradiation, significantly enhancing antimicrobial effects. Additionally, the study demonstrated promising biological applications for the new conjugates including radical scavenging activity, antidiabetic effects, DNA cleavage activity, and inhibition of biofilm formation by *S. aureus* and *P. aeruginosa*.

2.1.4. Photocatalytic applications. The potential of **Pc@CDs** to generate ROS is much lower in the context of photocatalytic applications than for phototherapeutic ones. However, some promising outcomes were achieved when the photooxidation of 4-chlorophenol was evaluated in the presence of unsymmetrical polystyrene membranes **ZnPc@NCDs-PS-membrane** bearing nanoassemblies consisting of non-substituted **ZnPc** and **CDs** with amino substituents (**NCDs**) covalently linked through an amide bond to carboxylated polystyrene (**CO_2H-PS**).[134] The synthetic strategy involved first the non-covalent conjugation of the unsubstituted **ZnPc** to the **NCDs**, obtained from the carbonization of citric acid and polyethyleneimine, according to previous works in the literature.[100,135] Subsequently, before membrane casting, the resulting **ZnPc@NCD** hybrid was covalently linked to **CO_2H-PS** *via* an amide bond using thionyl chloride to mediate the for-

Table 3 Summary of the properties of non-covalently bonded **Pc@CD** conjugates for antibacterial activity

CDs type	Chemical conjugation	Phthalocyanine	Φ_{CD}	Φ_{Pc}	Φ_{hybrid}	Application	Ref.
CDs	Non-covalent (π–π stacking)	2,9(10),16(17),23(24)-Tetrakis[[(phenoxy)ethan-1-one]phthalocyanine (**H_2Pc24**)	**CDs** (0.35)[a]	**H_2Pc24** (0.20)[a] **H_2Pc24** (0.31)[b] **H_2Pc24** (0.22)[c]	**H_2Pc24@CDs** (0.0.39)[a] **H_2Pc24@CDs** (0.27)[b] **H_2Pc24@CDs** (0.20)[c]	PDT against *S. aureus*	129
CDs	Non-covalent (π–π stacking)	2,9(10),16(17),23(24)-Tetrakis[[(phenoxy)ethan-1-one]phthalocyaninato zinc(II) (**ZnPc24**)	**CDs** (0.35)[a]	**ZnPc24** (0.13)[a] **ZnPc24** (0.78)[b] **ZnPc24** (0.72)[c]	**ZnPc24@CDs** (0.059)[a] **ZnPc24@CDs** (0.85)[b] **ZnPc24@CDs** (0.77)[c]	PDT against *S. aureus*	129
CDs	Non-covalent (π–π stacking)	2,9(10),16(17),23(24)-Tetrakis[[(phenoxy)ethan-1-one]phthalocyaninato indium(III) chloride (**InPc24**)	**CDs** (0.35)[a]	**InPc24** (0.046)[a] **InPc4** (0.84)[b] **InPc4** (0.75)[c]	**InPc24@CDs** (0.054)[b] **InPc24@CDs** (0.90)[b] **InPc24@CDs** (0.79)[c]	PDT against *S. aureus*	129
NCDs	Non-covalent (π–π stacking)	2,9(10),16(17),23(24)-Tetrakis[4-(4-(5-chloro-1*H*-benzo[*d*]imidazol-2-yl)phenoxy)]phthalocyaninato zinc(II) (**ZnPc25**)	**NCDs** (0.19)[d]	**ZnPc25** (0.17)[a]	**ZnPc25@NCDs** (0.12)[a]	PDT against *S. aureus*	132
CBDs	Non-covalent (π–π stacking)	1, 8(11),15(18),22(25)-Tetrakis[(2,2-dimethyl-1,3-dioxolan-4-yl)methoxy]phthalocyaninato copper (II)	—	—	—	PDT against Gram-positive bacteria (*E. hirae* and *E. faecalis*), Gram-negative bacteria (*E. coli*, *P. aeruginosa* and *B. subtilis*)	133

[a] Φ_f in DMSO. [b] Φ_T in DMSO. [c] Φ_Δ in DMSO. [d] Φ_f in H_2O.

mation of activated acyl chloride functionalities. This step was considered to avoid the leaching of ZnPc from the membrane, as observed when **ZnPc** or **ZnPc@NCDs** were simply mixed with the polymer solution (without prior conjugation). Then, the **ZnPc@NCDs-PS-membrane** was obtained by casting on glass slides a dispersion of non-functionalized polystyrene (PS) and the conjugate in DMF, followed by precipitation in a methanol bath.[134] The photophysical characterization confirmed the ability of the membranes to generate $^1O_2$ in ethanol (Φ_Δ = 0.43) and water (Φ_Δ = 0.37) *versus* **ZnPc@NCDs** (Φ_Δ = 0.49), allowing the photocatalytic oxidation of 4-chlorophenol in aqueous media. The study showed that the reaction followed second-order kinetics at 3.24×10^{-4} mol L^{-1} with a k_{obs} of 35.9 L mol^{-1} min^{-1} and a half-life of 86 min. Although the membrane was able to photodegrade 4-chlorophenol in water, its efficiency was not fully revealed.

A recent study explored the combination of CDs functionalized with **NiPc** and Cu–In–Zn–S quantum dots (**CIZS QDs**) for surface proton generation and reduction. The synthesis of the ternary **CIZS QD/NiPc@CD** composite is presented in Fig. 9A.[136] The size of the **CIZS QDs** and **CDs** was determined by transmission electron microscopy (TEM), corresponding to 3.5 ± 0.5 and 2.5 ± 0.5 nm, respectively (Fig. 9B and C). The nanocomposite **CIZS QDs/NiPc@CDs** revealed the formation of smaller **NiPc@CDs** and larger **CIZS QDs**. The HRTEM analysis of the **CIZSQDs/NiPc@CDs** confirms the presence of both nanostructures with lattice spacings of 0.310 nm, corresponding to the **CIZS QDs**, and 0.210 nm, corresponding to the CDs (Fig. 9D and E). Elemental mapping images of the **CIZS QDs/NiPc@CDs** further confirmed that In, Cu, Zn, S, Ni, and C were well merged, indicating that **CIZS QDs** and **NiPc@CDs** were well integrated to form the nanocomposite material (Fig. 9F-J). The performance of the developed ternary nanocomposites **CIZS QDs/NiPc@CDs** was evaluated in photocatalytic hydrogen evolution coupled with organic oxidation electron/hole extraction. A preliminary study, based on the photocatalytic degradation of rhodamine B (RhB), showed (Fig. 9K) that the **CIZS QD/NiPc@CD** nanocomposite presented higher photodegradation activity. The authors demonstrated that the dominant mechanism was based on photogenerated holes because with the addition of ethylenediaminetetraacetic acid (hole quencher), the photodegradation reaction was completely inhibited (Fig. 9I). This clearly illustrates that the photogenerated holes mainly contribute to the degradation of RhB in the **CIZS QD/NiPc@CD** composite photocatalyst system, which also proves the effectiveness of the hole-extraction strategy by **NiPc@CD** modification. The performance of the **CIZS/NiPc@CD** nanocomposite was further assessed for the photocatalytic hydrogen evolution coupled with the oxidation of different alcohols. The photocatalytic hydrogen production rate by **CIZS QDs/NiPc@CDs** *via* MeOH oxidation was found to be the highest among all the tested nanomaterials, reaching 1.121 mmol g^{-1} h^{-1} (Fig. 9M and N). Moreover, the oxidation of biomass-derived furfuryl alcohol (FFA) resulted in hydrogen production that reached 2.516 mmol g^{-1} h^{-1} (Fig. 9O and P).

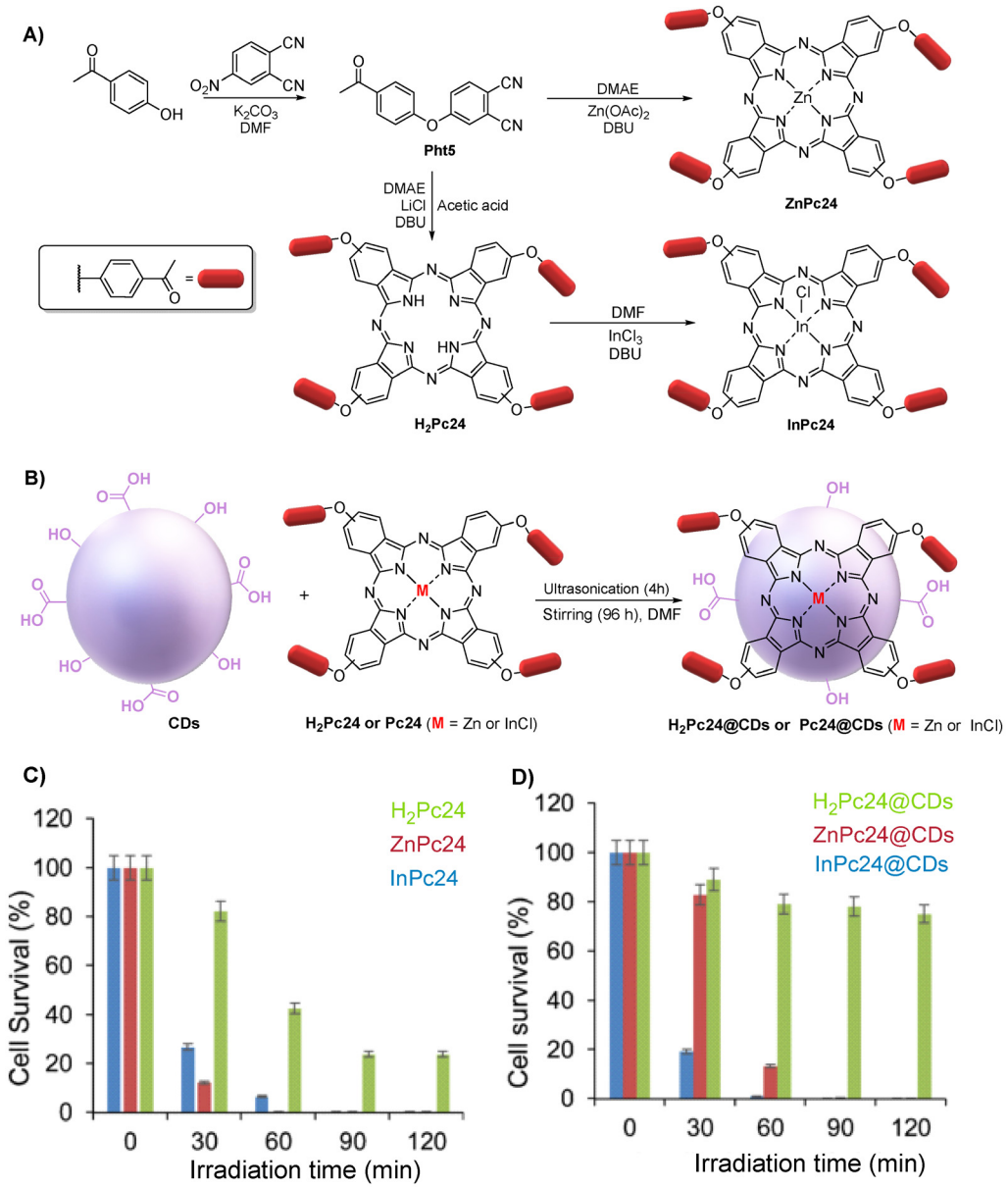

Fig. 8 (A) Synthesis of **H_2Pc24**, **ZnPc24**, and **InPc24** and (B) conjugation of Pcs with CDs. (C) Survival graphs of *S. aureus* incubated with 10 μM of photosensitizer for Pcs alone and for the conjugates (D) with irradiation at 670 nm. Reproduced with permission.[129] Copyright 2019, Elsevier B.V.

2.1.5. Miscellaneous applications. With future applications in molecular sensors and solar cells in mind, Majeed *et al.* studied the nonlinear optical responses of carbazole-substituted ZnPc (**ZnPc26A-C**) conjugated to CDs and in thin films (TF) of polystyrene (PS) (Fig. 10).[137] These **ZnPcs** were obtained by tetramerization of suitable phthalonitriles in quinolone at 80 °C in the presence of anhydrous $Zn(OAc)_2$ and DBU. **Phts 6A-C** were prepared from the reaction of commercially available 4,5-dichlorophthalonitrile with the required carbazoles in dry DMF in the presence of cesium fluoride.

The immobilization of the ZnPc in CDs obtained from the pyrolysis of citric acid in the presence of NaOH afforded the required nanoassemblies **ZnPc26A-C@CDs** that after being embedded in PS films showed an average thickness of 0.45–0.62 mm. These thin films of **ZnPc26A-C@CDs-PS** showed promising optical limiting parameters in different solvents, with improved optical limiting performance, characterized by increased third-order susceptibilities and hyperpolarizabilities, as well as lower limiting threshold values.

In 2021, AlMarzouq *et al.* selected the analogue manganese phthalocyanine with eight carbazole units (**MnPc26C**) to conjugate with CDs, which were obtained through the pyrolysis of calcium acetate at 200 °C, to evaluate the influence of the carbazole substituents and CDs on the redox mechanism of MnPc.[138] The electrochemical performance of **MnPc26C** and the resulting conjugate was investigated using

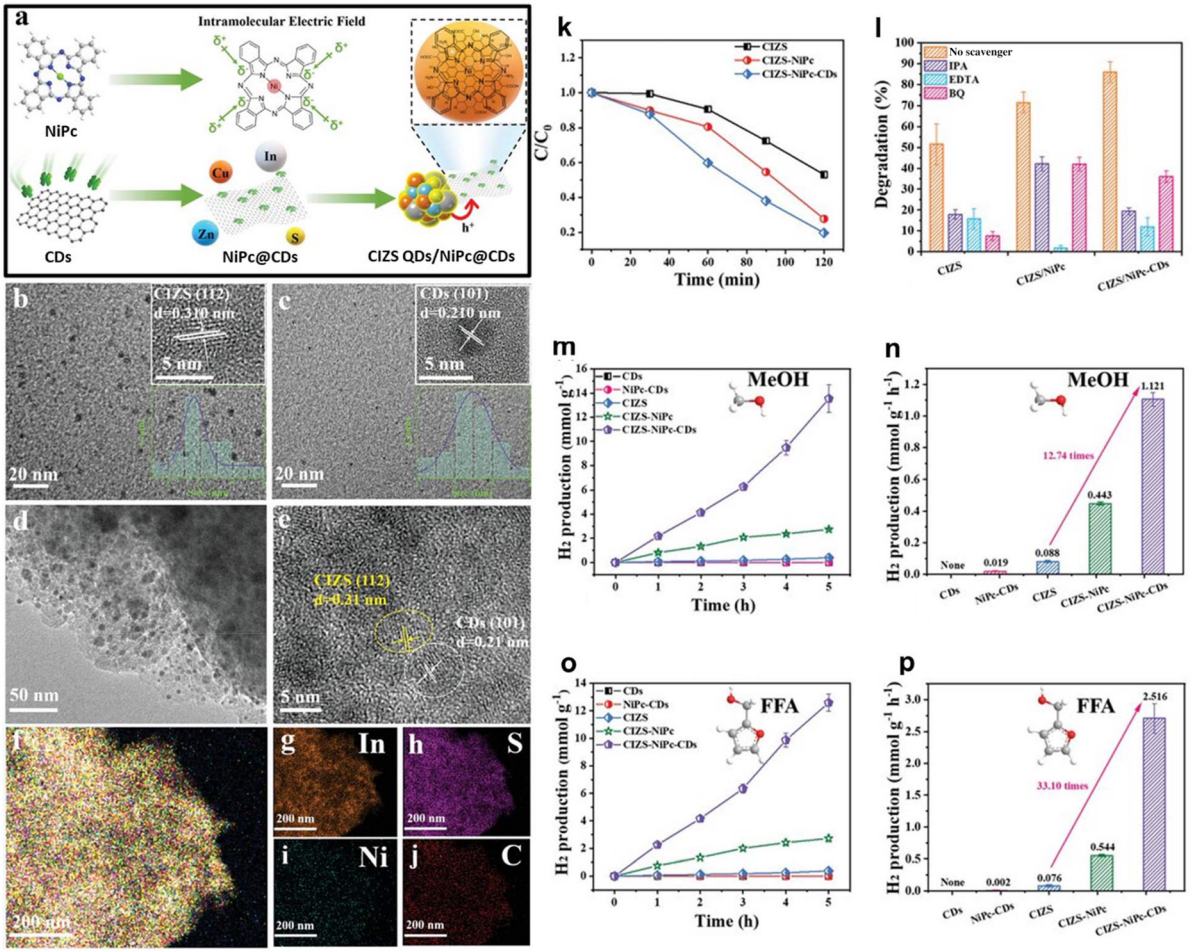

Fig. 9 (a) Schematic diagram for the construction of the ternary **CIZS QD/NiPc@CD** composite. (b) TEM images of **CIZS QDs** and (c) **CDs** and the corresponding HRTEM images (top insets) and size distribution histograms (bottom insets) obtained by counting 100 particles. (d) TEM and (e) HRTEM images of **CIZS QDs/NiPc@CDs**. (f–j) The corresponding elemental mapping images of **CIZS QDs/NiPc@CDs**. (k) Photocatalytic degradation ratio of RhB over **CIZS QDs**, **CIZS QDs/NiPc**, and **CIZS QDs/NiPc@CDs** under visible-light irradiation. (l) Active species trapping experiment during the photocatalytic degradation of RhB over **CIZS QDs/NiPc@CDs** with the addition of quenchers of h^+ (EDTA), $^{\bullet}O^{2-}$ (BQ), and $^{\bullet}OH$ (isopropanol, IPA). Photocatalytic hydrogen evolution performance over **CDs**, **NiPc@CDs**, **CIZS QDs**, **CIZS QDs/NiPc**, and **CIZS QDs/NiPc@CDs** coupled with (m), (n) methanol oxidation and (o and p) FFA oxidation reactions. Reproduced with permission.[136] Copyright 2023, John Wiley & Sons, Inc.

cyclic voltammetry (CV), square wave voltammetry (SWV), and spectroelectrochemistry (SEC), showing extended metal-based redox processes at low potentials. Furthermore, the carbazole substituents provided additional redox activity, facilitating the electropolymerization of the complex onto the electrode surface, simplifying the electrode modification.

2.2. Covalent functionalization

2.2.1. Fundamental insights into Pc@CDs' features. The covalent functionalization of the CDs with Pcs has been significantly less explored compared to the non-covalent approach. However, some different applications can be found in the literature and are summarized in Table 4. One of the most relevant advantages of exploring the covalent bond is the stability of the conjugate. The most common approaches for establishing stable covalent bonds between CDs and Pcs generally involve esterification or amidation reactions. In 2020, Prato *et al.* developed the **ZnPc27@NCD** hybrid by linking the amorphous NCDs to the non-symmetric **ZnPc27** *via* an amide bond (Fig. 11A).[139] This dye acted as an electron donor with a large extended π-surface and strong absorption in the visible spectrum. Intermolecular interactions were confirmed by steady-state and pump–probe transient absorption spectroscopy, which revealed symmetry-breaking charge transfer/separation and recombination dynamics within pairs of Pcs. Moreover, steady-state fluorescence experiments showed quenching in the formed hybrid material, accompanied by a red shift of the fluorescence maximum, upon excitation at λ = 387 nm (Fig. 11A). The CDs simplify the electronic interactions between the studied Pcs, suggesting that they can be used to support electronic couplings in multichromophoric arrays, which can increase their application in organic electronics, photonics, and/or artificial photosynthesis systems. Examples

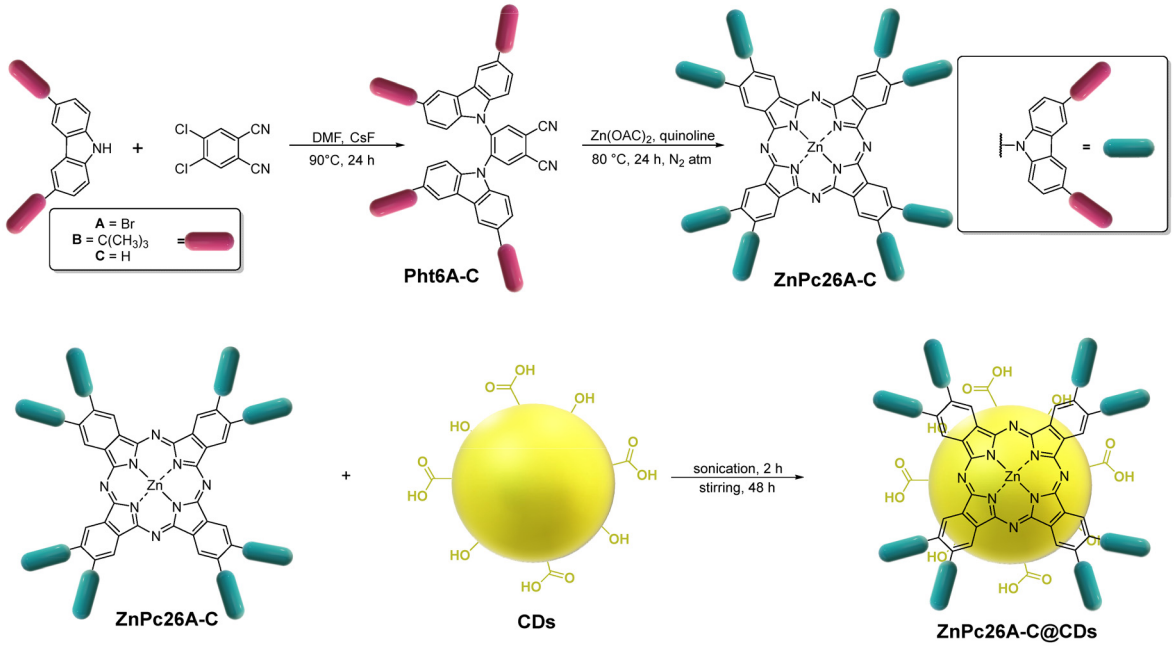

Fig. 10 Preparation of **ZnPc26A-C** substituted with eight carbazole units used in the synthesis of **ZnPc26A-C@CD** nanoassemblies further immobilized in polystyrene films.[137]

of this type of conjugation and their respective potential applications are discussed in the following sections.

2.2.2. Electrocatalytic applications. The possibility of using CDs in the oxygen reduction reaction (ORR) merits special attention from the scientific community because of their efficiency in lowering the oxygen adsorption and first electron transfer barriers and consequently providing enhanced electrocatalytic activity.[143] This reaction plays an important role in fuel cells and metal–air batteries, and although Pt-based nanomaterials display excellent activities for the ORR, their high cost and poor durability limit their wide application. Thus, CDs can be an excellent alternative, although some drawbacks, such as low limiting current density and potential onset, still require improvement. Based on the knowledge that the hybridization of CDs with other functional materials is a potential strategy for improving their ORR catalytic properties, Koh *et al.* were prompted in 2017 to evaluate the ORR electrocatalytic activity of **FePc@CD** conjugates obtained through the coordination of the metal ion in **FePc** to the CDs.[144] In the selection of **FePc**, the authors considered its efficiency as an electrocatalyst for the ORR. The CDs were obtained by the hydrothermal treatment of GO using NH_4OH and H_2O_2. The immobilization of FePc on the CDs was performed at room temperature in DMSO and pyridine, and the color change from blue to green confirmed the successful coordination of the metal to the CDs. The results from the electrochemical assays showed a higher performance of **FePc@CDs** when compared with CDs, and a Pt/C electrode was selected for comparison. All samples in O_2-saturated electrolyte exhibited cathodic current peaks in contrast to the assays performed in N_2 that exhibited only very weak cathodic current peaks due to intrinsic redox.[145] The positive shift of the ORR peak of **FePc@CDs** (0.1 V *vs.* Hg/HgO) when compared with the CD peak (0.18 V *vs.* Hg/HgO) and the two times higher oxygen reduction current of the conjugate was justified to be mainly due to the charge transfer behaviour from CDs to electronegative **FePc**. The results showed that **FePc@CDs**, like the Pt/C electrode, mediated the desired four-electron reaction in an alkaline electrolyte, in contrast to CDs, which presented a two-electron transfer process yielding HO_2^-. Other positive outcomes compared to Pt/C are a higher limiting current density, excellent methanol tolerance, insensitivity to CO poisoning, and electrochemical stability. Thus, **FePc@CDs** have the potential to be used as efficient nonprecious electrocatalysts for the ORR and may be used in commercial applications of fuel cells.

Knowing that the elimination of oxygen-containing groups from the surface of CDs is responsible for reducing the energy band gap of reduced carbon dots (**rCDs**) compared to amino-functionalized CDs (**NCDs**), resulting in materials with improved electron transfer processes and conductivity, Centane *et al.*[141] developed conjugates based on **CoPc28** (Fig. 11B) covalently linked to **NCDs** and **rCDs** and evaluated their performance during the electrocatalysis of hydrazine on a glassy carbon electrode (GCE). For comparison, the authors also considered the development of analogous nanoassemblies obtained *via* π–π interactions. Unsymmetrical **CoPc28** was obtained by the condensation of 4-(*p-tert*-butylphenoxy)phthalonitrile (**Pht7**) and 4-(4-carboxyphenoxy)phthalonitrile in pentanol at 160 °C and in the presence of $CoCl_2{\cdot}6H_2O$ and DBU (**CoPc28**, Fig. 11C).[140] NCDs were synthesized by oxidative cutting of GO sheets with $KMnO_4$ and H_2SO_4, followed by the reaction of the obtained CDs with an ammonia solution in the

Table 4 Summary of the properties and applications of covalently bonded **Pc@CD** conjugates

CDs type	Chemical conjugation	Phthalocyanine	Φ_{CD}	Φ_{Pc}	Φ_{Hybrid}	Application	Ref.
NCDs	Covalent	9(10),16(17),23(24)-Tri-*tert*-butyl-2-carboxy-5,28 : 14,19-diimino-7,12 : 21,26-dinitrilotetrabenzo[*c*,*h*,*m*,*r*][1,6,11,16] tetraazacycloeicosinato-(2$^-$)-N^{29},N^{30},N^{31},N^{32} zinc(II) (**ZnPc27**)	**NCDs** (0.17)[a]	**ZnPc27** (0.15)[a]	*	Charge transfer	139
CDs, rCDs and **NCDs**	Covalent and/or non-covalent (π–π stacking)	2-Mono[(4-carboxyphenoxy)]-9(10),16(17),23(24)-Tris[*tert*-butylphenoxy]phthalocyaninato cobalt(II) (**CoPc28**)	*	*	*	Electrooxidation of hydrazine	141
NCDs	Covalent and/or non-covalent (π–π stacking)	2-Mono[(4-carboxyphenoxy)]-9(10),16(17),23(24)-Tris[phenyl] phthalocyaninato zinc(II) (**ZnPc29**)	**NCDs** (0.16)[a]	**ZnPc29** (0.16)[a] **ZnPc29** (0.70)[b] **ZnPc29** (0.56)[c]	**πZnPc29@NCDs** (0.18)[a] **πZnPc29@NCDs** (0.70)[b] **πZnPc29@NCDs** (0.33)[c] **ZnPc29@NCDs** (0.19)[a] **ZnPc29@NCDs** (0.49)[b] **ZnPc29@NCDs** (0.44)[c]	Determination of Φ_Δ values	140
NCDs	Covalent	2,9(10),16(17),23(24)-Tetrakis[(3-carboxyphenoxy)] phthalocyaninato cobalt(II) (**CoPc30**)	*	*	*	Electrochemical sensors for dopamine, norepinephrine, and epinephrine detection	142

[a] Φ_f in DMSO. [b] Φ_T in DMSO. [c] Φ_Δ in DMSO.

presence of EDC/*N*-hydroxysuccinimide (NHS). On the other hand, rCDs were obtained by treating the CDs in water with hydrazine hydrate to eliminate the high number of oxygen-containing functionalities. The **CoPc28@rCDs** and **CoPc28@NCDs** hybrids were obtained by reacting **CoPc28** and the required CDs in DMF and using EDC/NHS as activating carboxyl reagents. The analogous π–π hybrids (**CoP28(π–π)@rCDs** and **CoPc28(π–π)@NCDs**) were obtained by sonication of the required constituents. The efficiencies of the precursors and conjugates covalently and non-covalently linked in the electrocatalysis of hydrazine were evaluated using a GCE. The procedure was conducted by placing each hybrid on the GCE, followed by drying at 70 °C to obtain the following electrodes: **CoPc28@GCE/rCDs**, **CoPc28@GCE/NCDs**, **CoPc28(π–π)@GCE/rCDs**, and **CoPc28(π–π)GCE/NCDs**. The **rCDs@GCE**, **NCDs@GCE**, and **CoPc@GCE** electrodes were prepared by the same procedure. Low LOD values for hydrazine oxidation were obtained in the presence of electrodes containing the hybrids prepared by covalent conjugation, **CoPc28@GCE/rCDs** and **CoPc28@GCE/NCDs**. It was also observed that the hybrids composed of rCDs gave better LOD values than the corresponding NCD hybrids. The results obtained confirmed that the elimination of excessive oxygen-containing groups from the surface of the CDs does indeed tune the energy band gap, improving the required electron transfer and conductivity.

To compare how the efficiency of a Pc at generating $^1O_2$ was affected by the type of bond linked to the CDs, Nyokong *et al.* (2019) developed polystyrene membranes **[ZnPc29@NCDs@PSCO$_2$H]$_m$** bearing **NCDs** covalently linked to the unsymmetrical **ZnPc29** bearing a carboxyphenoxy unit and to carboxyl-functionalized polystyrene ($PSCO_2H$) through amide bonds; membranes resulting from the π–π interactions between **ZnPc29** and **NCDs@PSCO$_2$H** were also prepared, **[πZnPc29@NCDs@PSCO$_2$H]$_m$** (Fig. 11B).[141] The NCDs were obtained through the hydrothermal treatment of GO with ammonia, and during the covalent conjugation process, their coupling with **ZnPc29** and then to $PSCO_2H$ was performed in DMF in the presence of DCC. The observation of shifts in the region of the amide peak in the FTIR spectra, from 1667 cm^{-1} in **ZnPc29@NCDs** to 1657 cm^{-1} in **ZnPc29@NCDs-(COOH)-PS**, suggested successful conjugation. Initially, the NCDs were monodispersed with a size of approximately 14 nm, but after conjugate formation, the size increased to 21 nm. The XRD diffractograms showed that the synthesized nanoconjugates were amorphous, like their constituents. Photophysical/photochemical characterization revealed that the hybrid materials exhibited better performance prior to incorporation into the membranes (*e.g.*, Φ_Δ of 0.33 (π) and 0.44 (c) compared to 0.16 (π) and 0.29 (c) after incorporation). Moreover, hybrids with covalent linkages consistently outperformed those with π–π interactions under both conditions.

2.2.3. Sensing applications. In 2022, Mashazi *et al.* developed an electrochemical sensor for the detection of catecholamine neurotransmitters using composites of **CoPc30** (Table 4) and aminated CDs (NCDs), covalently functionalized onto an isophthalic acid electrografted gold electrode (Au-IPA).[142] The electrochemical performance of the composite-modified gold

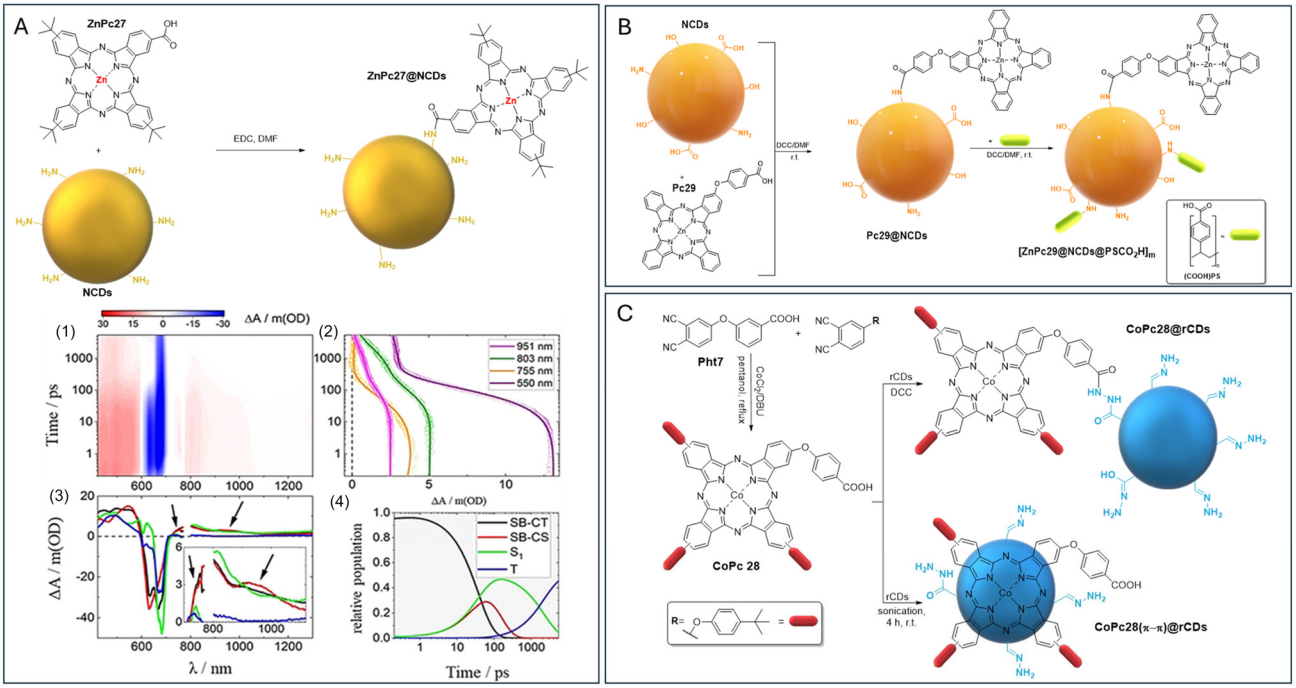

Fig. 11 (A) NCDs covalently linked to **ZnPc27**: (1) differential absorption 3D map obtained by fsTAS of **ZnPc27@NCDs** in CH_3OH at room temperature upon excitation at λ = 387 nm; (2) time absorption profiles and the corresponding line fittings at λ = 951 (magenta), 803 (dark green), 755 (orange), and 550 nm (purple); (3) species-associated differential spectra of SB-CT (black), SB-CS (red), S1 (green), and T1 (blue) excited states; and (4) concentration evolution over time.[139] (B) Synthesis of **CoPc28** and its functionalization with **rCDs** to obtain **CoPc28@rCD** and **CoP28(π–π)@rCD** hybrids.[140] (C) Strategy used in the preparation of a **[ZnPc29@NCDs@PSCO$_2$H]$_m$** membrane.[141]

surface was evaluated using CV, differential pulse voltammetry (DPV), SWV, and electrochemical impedance spectroscopy (EIS) in PBS and newborn calf serum (NCS). The sensor demonstrated improved electrochemical performance for detecting dopamine (DA), epinephrine (EP), and norepinephrine (NR), with broad linear ranges (1.0–50 μM in PBS and 0.0–60 μM in serum) and low detection limits in the μM range. Moreover, the engineered electrochemical sensor exhibited an interesting capability to suppress background current and was effectively used for the detection of catecholamine neurotransmitters in newborn calf serum with high recovery.

3. Conclusions

CDs have emerged as versatile nanoplatforms capable of addressing key limitations associated with molecular compounds such as Pcs. By combining CDs with Pcs, the resulting hybrid macrocycles exhibit improved light sensitivity, water solubility, stability, and environmental compatibility. This review allows us to conclude that this integration can significantly expand the applications of Pcs, with the resulting hybrids showing great promise in diverse fields, including biosensing, phototherapeutic applications, photocatalysis, electrocatalysis, and oxygen reduction reactions (ORRs) among others.

Most of the research focused on developing Pcs and CDs with compatible functionalities. This involved tailoring the structural features of Pcs, such as peripheral substituents (α and/or β), varying the types and number of functional groups, and modulating charge distributions (neutral, positive, or negative). These modifications enabled the resulting hybrids to achieve in general appropriate performance in terms of Φ_Δ, Φ_F, photostability, hydrophilicity, and targeted functionality.

The conjugation of CDs with Pc dyes through covalent or non-covalent interactions yielded Pc@CD hybrids with distinct photophysical properties. Covalent strategies were primarily based on amidation and esterification. The wide structural variety of Pcs facilitated the functionalization of oxygen and nitrogen-containing groups on the CDs. While covalently bonded hybrids exhibit greater chemical stability and higher reaction yields, their practical applications are hindered by synthetic complexity, generally requiring the preparation of non-symmetrical Pcs. Nevertheless, covalent functionalization influences the interaction between the two structures, modulating photoluminescence, preserving the capacity for $^1O_2$ generation and introducing interesting features favorable for mediating electron transfer, conductivity and ORR processes. Although the number of reported examples is limited, we believe that continued efforts to develop these types of hybrids can significantly impact renewable energy technologies, advance environmental sustainability, improve catalytic efficiency, and drive innovations in therapeutic applications. On the other hand, non-covalent conjugation, achieved through electrostatic interactions, complexation, or π–π stack-

ing, facilitates the easy formation of supramolecular structures. Considering that some Pc@CD hybrids exhibit pH-dependent behavior, some groups were prompted to explore electrostatic interactions to optimize Pc–CD binding. The non-covalent conjugation approach offers the advantage of faster and simpler reaction steps while preserving the structural and electronic characteristics of the starting materials. However, non-covalent strategies generally compromise the photoluminescence of Pc@CD hybrids due to quenching effects. These quenching effects were extensively explored in sensing applications, where luminescence was recovered upon interaction with the target analyte.

Despite the observed decrease in the fluorescence quantum yield (Φ_F) of the conjugates and the corresponding increase in triplet quantum yield (Φ_T), these changes did not always translate into improved efficiency in generating $^1O_2$ due to competing screening processes that reduce light absorption or oxygen access to the active sites of the photosensitizer. Nevertheless, depending on the structural features of the Pcs, these limitations were overcome in some cases, leading to promising outcomes in PDT and aPDT. The ability to generate ROS was also explored in oxidative processes in water, although the number of studies remains very limited. Similarly, studies related to hydrogen production are scarce.

Despite significant progress, the development of highly efficient Pc@CD hybrids remains an open research frontier. The primary challenge lies in mitigating the partial or total quenching of Pcs by CDs, an effect observed in both covalent and non-covalent conjugation approaches. This quenching typically results in reduced Φ_F values and ROS production, primarily due to Förster resonance energy transfer (FRET), when compared to free-base Pcs. A critical question to address this issue is how to prevent planar coupling between CDs and Pcs. One promising approach involves the exploration of metalated phthalocyanines with bulky aromatic or aliphatic substituents linked by N, O, or S atoms at the peripheral positions (α- and/or β-). These substituents can introduce steric hindrance to aromatic CDs, thereby minimizing quenching effects. Also, the metalation of Pcs with transition metals that require axial ligands, such as In^{3+}, Ga^{3+}, or Si^{4+}, can further minimize the direct contact between CDs and Pcs, enhancing the overall performance of the hybrid systems.

Another important aspect is the wide range of synthetic approaches and precursors available to produce CDs in the development of Pc@CD hybrids, which significantly influence their structural and photophysical/photochemical properties. Therefore, ensuring reproducibility and scalability remains a critical challenge. To address this, it is essential to have well-documented and standardized synthetic protocols that provide clear details on reaction conditions, precursor ratios, and processing steps. This will promote reproducibility and comparability across studies. Advanced characterization techniques and quality control measures will also be vital for confirming structural integrity and performance. In this context, emerging technologies like machine learning (ML) and deep learning (DL) can offer powerful tools for the optimization and automated identification of new synthetic conditions. By analyzing large datasets, ML and DL can identify patterns, predict material properties, optimize the process and ultimately enable more efficient synthetic protocols. These approaches have the potential to significantly enhance the performance of these hybrids, unlocking new possibilities for their applications across diverse fields.

Abbreviations

0D	Zero dimensional
$^1O_2$	Singlet oxygen
2D	Two dimensional
6FBPA	Bisphenol A hexafluoride
AA	Ascorbic acid
AFM	Atomic force microscopy
AmGQDs	Aminated graphene quantum dots
aPDT	Antimicrobial photodynamic therapy
Au-IPA	Isophthalic electrografted gold electrode
CDs	Carbon dots
CNPs	Carbonized nanoparticles
CNTs	Carbon nanotubes
CPDs	Carbonized polymer dots
CQDs	Carbon quantum dots
CV	Cyclic voltammetry
DA	Dopamine
DBN	1,8-Diazabicyclo[5.4.0]undec-7-ene (DBU) or 1,5-diazabicyclo[4.3.0]non-5-ene
DBU	1,8-Diazabicyclo[5.4.0]undec-7-ene
DCC	*N*,*N*′-Dicyclohexylcarbodiimide
DMAE	2-Dimethylaminoethanol
DMAP	4-Dimethylaminopyridine
DMF	*N*,*N*′-dimethylformamide
DMMP	Methylphosphonate
DMSO	Dimethyl sulfoxide
DPV	Differential pulse voltammetry
ds-DNA	Double-stranded DNA
EDC	1-Ethyl-3-(3-dimethylaminopropyl)carbodiimide
EIS	Electrochemical impedance spectroscopy
EP	Epinephrine
EPR	Enhanced permeation retention
FRET	Förster resonance energy transfer
FTIR	Fourier transform infrared spectroscopy
GCE	Glassy carbon electrode
GO	Graphene oxide
GQDs	Graphene quantum dots
H_2Pc	Free-base phthalocyanine
HFIP	hexafluoroisopropanol
ICT	Inter-charge transfer
IPCA	5-Oxo-1,2,3,5-tetrahydroimidazo-[1,2-α]-pyridine-7-carboxylic acid
LOD	Limit of detection
MCF-7 cell lines	Human breast cancer cell lines
MPc	Metalophthalocyanine

MW	Microwave treatment
NCNDs	N-doped carbon nanodots
NCDs	Nitrogen doped-carbon dots
NHS	*N*-Hydroxysuccinimide
NMR	Nuclear magnetic resonance
NOR	Norepinephrine
NSCDs	Nitrogen–sulfur doped-carbon dots
ORR	Oxygen reduction reaction
PACT	Photodynamic antimicrobial chemotherapy
PBS	Phosphate-buffered saline
Pc(s)	Phthalocyanine(s)
PDT	Photodynamic therapy
PET	Photo-induced electron transfer
PL	Photoluminescence
Por	Porphyrin
QY	Quantum yield
rGQDs	Reduced graphene quantum dots
SDT	Sonodynamic therapy
SEC	Spectroelectrochemistry
SEM	Scanning electron microscopy
SWV	Square wave voltammetry
t-CDs	Thermally-reduced carbon dots
TEM	Transmission electron microscopy
TEMPOL	(4-Hydroxy-2,2,6,6-tetramethylpiperidine-1-oxyl 2,2,6,6-tetramethylpiperidin-1-yl)oxyl
TEMPO-Pht	Phthalonitrile bearing the radical scavenger TEMPOL
XPS	X-ray photoelectron spectroscopy
XRD	X-ray diffraction
J	Spectral overlap
τ_f	Fluorescence lifetime
Φ_F	Fluorescence quantum yield
Φ_{PL}	Photoluminescence quantum yield
Φ_T	Triplet quantum yield
Φ_Δ	Singlet oxygen quantum yield

Data availability

No primary research results, software or code have been included and no new data were generated or analysed as part of this review.

Conflicts of interest

There are no conflicts to declare.

Acknowledgements

Authors acknowledge to University of Aveiro, Instituto Superior Técnico (IST, Portugal) and FCT/MCTES (Fundação para a Ciência e Tecnologia/Ministério da Ciência e Tecnologia, Portugal) for the support to LAQV-REQUIMTE and CQE-IST to the project: 2022.05950.PTDC (**https://doi.org/10.54499/2022.05950.PTDC**) through national funds, where applicable, co-financed by European Union, FEDER, QREN, and COMPETE within the PT2020 Partnership Agreement, and to the Portuguese NMR Network. C. I. M. Santos is also grateful to her research contract (REF.IST-ID/95/2018, 2023.08400. CEECIND). Funding: This research work received financial support from Instituto Superior Técnico (IST, Portugal), the University of Aveiro and FCT/MCTES (Fundação para a Ciência e Tecnologia (FCT) and Ministério da Ciência Tecnologia e Ensino Superior) to support the LAQV-REQUIMTE (LA/P/0008/2020 **https://doi.org/10.54499/LA/P/0008/2020,** UIDP/50006/2020 **https://doi.org/10.54499/UIDP/50006/2020** and UIDB/50006/2020 **https://doi.org/10.54499/UIDB/50006/2020**), by IMS (LA/P/0056/2020, **https://doi.org/10.54499/LA/P/0056/2020**), CQE (UIDB/00100/2020, **https://doi.org/10.54499/UIDP/00100/2020** and UIDP/00100/2020, **https://doi.org/10.54499/UIDP/00100/2020**), and TEMA (UIDB/00481/2020 **https://doi.org/10.54499/UIDB/00481/2020** and UIDP/00481/2020 **https://doi.org/10.54499/UIDP/00481/2020**), research units through national funds and was co-financed by the FEDER, within the PT2020 Partnership Agreement, and to the Portuguese NMR Network. The authors also thanks to the FCT for the financial support of the project CarboNCT - 2022.03596.PTDC (**https://doi.org/10.54499/2022.03596.PTDC**).

References

1 M. W. Jones, A. I. Coppola, S. H. Doerr, T. A. Quine, C. Santín, T. Dittmar and R. Jaffé, *Nat. Commun.*, 2020, **11**, 1.
2 Z. Zhao, W. Zhang, J. Zhang, Y. Li, H. Bai, F. Zhao, Z. Jin, J. Tang, Y. Xiao, W. Xu and Y. Lü, *Adv. Photonics Res.*, 2024, **5**, 2400010.
3 Q. Xu, W. Li, L. Ding, W. Yang, H. Xiao and W. Ong, *Nanoscale*, 2019, **11**, 1475.
4 K. Jiang, S. Sun, L. Zhang, Y. Lu, A. Wu, C. Cai and H. Lin, *Angew. Chem.*, 2015, **127**, 5450.
5 L. Đorđević, F. Arcudi, M. Cacioppo and M. Prato, *Nat. Nanotechnol.*, 2022, **17**, 112.
6 A. Das, E. V. Kundelev, A. A. Vedernikova, S. A. Cherevkov, D. V. Danilov, A. V. Koroleva, E. V. Zhizhin, A. N. Tsypkin, A. P. Litvin, A. V. Baranov, A. V. Fedorov, E. V. Ushakova and A. L. Rogach, *Light:Sci. Appl.*, 2022, **11**, 1.
7 Q. Zhang, R. Wang, B. Feng, X. Zhong and K. (Ken) Ostrikov, *Nat. Commun.*, 2021, **12**, 1.
8 B. Bartolomei, A. Bogo, F. Amato, G. Ragazzon and M. Prato, *Angew. Chem., Int. Ed.*, 2022, **61**, e202200038.
9 S. Hu, A. Trinchi, P. Atkin and I. Cole, *Angew. Chem., Int. Ed.*, 2015, **54**, 2970.
10 G. E. Lecroy, F. Messina, A. Sciortino, C. E. Bunker, P. Wang, K. A. S. Fernando and Y. P. Sun, *J. Phys. Chem. C*, 2017, **121**, 28180.
11 F. Yan, Z. Sun, H. Zhang, X. Sun, Y. Jiang and Z. Bai, *Microchim. Acta*, 2019, **186**, 1.
12 H. Ali, S. Ghosh and N. R. Jana, *Wiley Interdiscip. Rev.: Nanomed. Nanobiotechnol.*, 2020, **12**, e1617.

13 J. Zhu and S. Mu, *Adv. Funct. Mater.*, 2020, **30**, 2001097.
14 Y. P. Sun, B. Zhou, Y. Lin, W. Wang, K. A. S. Fernando, P. Pathak, M. J. Meziani, B. A. Harruff, X. Wang, H. Wang, P. G. Luo, H. Yang, M. E. Kose, B. Chen, L. M. Veca and S. Y. Xie, *J. Am. Chem. Soc.*, 2006, **128**, 7756.
15 X. T. Tian and X. B. Yin, *Small*, 2019, **15**, 1901803.
16 Z. Wang, F. Yuan, X. Li, Y. Li, H. Zhong, L. Fan and S. Yang, *Adv. Mater.*, 2017, **29**, 1702910.
17 D. Li, P. Jing, L. Sun, Y. An, X. Shan, X. Lu, D. Zhou, D. Han, D. Shen, Y. Zhai, S. Qu, R. Zbořil and A. L. Rogach, *Adv. Mater.*, 2018, **30**, 1705913.
18 M. T. Hasan, R. Gonzalez-Rodriguez, C. Ryan, N. Faerber, J. L. Coffer and A. V. Naumov, *Adv. Funct. Mater.*, 2018, **28**, 1804337.
19 B. Ju, H. Nie, Z. Liu, H. Xu, M. Li, C. Wu, H. Wang and S. X. A. Zhang, *Nanoscale*, 2017, **9**, 13326.
20 H. Nie, M. Li, Q. Li, S. Liang, Y. Tan, L. Sheng, W. Shi and S. X. A. Zhang, *Chem. Mater.*, 2014, **26**, 3104.
21 H. Ding, J. S. Wei, P. Zhang, Z. Y. Zhou, Q. Y. Gao and H. M. Xiong, *Small*, 2018, **14**, 1800612.
22 S. Miao, K. Liang, J. Zhu, B. Yang, D. Zhao and B. Kong, *Nano Today*, 2020, **33**, 100879.
23 X. Li, Y. Fu, S. Zhao, J. F. Xiao, M. Lan, B. Wang, K. Zhang, X. Song and L. Zeng, *Chem. Eng. J.*, 2022, **430**, 133101.
24 S. Yoo, Y. Song and S. Hahn, *Light:Sci. Appl.*, 2022, **11**, 1.
25 J. Tang, J. Zhang, Y. Zhang, Y. Xiao, Y. Shi, Y. Chen, L. Ding and W. Xu, *Nanoscale Res. Lett.*, 2019, **14**, 1.
26 M. Bottrill and M. Green, *Chem. Commun.*, 2011, **47**, 7039.
27 K. M. Tsoi, Q. Dai, B. A. Alman and W. C. W. Chan, *Acc. Chem. Res.*, 2013, **46**, 662.
28 L. Ye, K. T. Yong, L. Liu, I. Roy, R. Hu, J. Zhu, H. Cai, W. C. Law, J. Liu, K. Wang, J. Liu, Y. Liu, Y. Hu, X. Zhang, M. T. Swihart and P. N. Prasad, *Nat. Nanotechnol.*, 2012, **7**, 453.
29 A. M. Derfus, W. C. W. Chan and S. N. Bhatia, *Nano Lett.*, 2004, **4**, 11.
30 Z. L. Wu, Z. X. Liu and Y. H. Yuan, *J. Mater. Chem. B*, 2017, **5**, 3794.
31 F. Arcudi, L. Ďorďević and M. Prato, *Acc. Chem. Res.*, 2019, **52**, 2070.
32 F. Arcudi, L. Đorđević, F. Arcudi and L. Đorđević, *Small*, 2023, **19**, 2300906.
33 L. Đorđević, F. Arcudi and M. Prato, *Nat. Protoc.*, 2019, **14**, 2931.
34 Y. Dong, J. Shao, C. Chen, H. Li, R. Wang, Y. Chi, X. Lin and G. Chen, *Carbon*, 2012, **50**, 4738.
35 I. L. Medintz, H. T. Uyeda, E. R. Goldman and H. Mattoussi, *Nat. Mater.*, 2005, **4**, 435.
36 H. Zhu, X. Wang, Y. Li, Z. Wang, F. Yang and X. Yang, *Chem. Commun.*, 2009, 5118.
37 H. Peng and J. Travas-Sejdic, *Chem. Mater.*, 2009, **21**, 5563.
38 D. V. Talapin, A. L. Rogach, E. V. Shevchenko, A. Kornowski, M. Haase and H. Weller, *J. Am. Chem. Soc.*, 2002, **124**, 5782.
39 Y. Yan, D. Zhai, Y. Liu, J. Gong, J. Chen, P. Zan, Z. Zeng, S. Li and W. Huang, *ACS Nano*, 2018, **12**, 3523.
40 J. Schneider, C. J. Reckmeier, Y. Xiong, M. Von Seckendorff, A. S. Susha, P. Kasak and A. L. Rogach, *J. Phys. Chem. C*, 2017, **121**, 2014.
41 F. Yuan, Y. K. Wang, G. Sharma, Y. Dong, X. Zheng, P. Li, A. Johnston, G. Bappi, J. Z. Fan, H. Kung, B. Chen, M. I. Saidaminov, K. Singh, O. Voznyy, O. M. Bakr, Z. H. Lu and E. H. Sargent, *Nat. Photonics*, 2019, **14**, 171.
42 L. Wang, Y. Wang, T. Xu, H. Liao, C. Yao, Y. Liu, Z. Li, Z. Chen, D. Pan, L. Sun and M. Wu, *Nat. Commun.*, 2014, **5**, 1.
43 E. Haque, J. Kim, V. Malgras, K. R. Reddy, A. C. Ward, J. You, Y. Bando, M. S. A. Hossain and Y. Yamauchi, *Small Methods*, 2018, **2**, 1800050.
44 C. I. M. Santos, I. F. A. Mariz, S. N. Pinto, G. Gonçalves, I. Bdikin, P. A. A. P. Marques, M. G. P. M. S. Neves, J. M. G. Martinho and E. M. S. Maçôas, *Nanoscale*, 2018, **10**, 12505.
45 C. I. M. Santos, L. Rodríguez-Pérez, G. Gonçalves, S. N. Pinto, M. Melle-Franco, P. A. A. P. Marques, M. A. F. Faustino, M.Á Herranz, N. Martin, M. G. P. M. S. Neves, J. M. G. Martinho and E. M. S. Maçôas, *Carbon*, 2020, **166**, 164.
46 C. I. M. Santos, L. Rodríguez-Pérez, G. Gonçalves, C. J. Dias, F. Monteiro, M. D. A. F. Faustino, S. I. Vieira, L. A. Helguero, M.Á Herranz, N. Martín, M. G. P. M. S. Neves, J. M. G. Martinho and E. M. S. Maçôas, *ACS Appl. Nano Mater.*, 2021, **4**, 13079.
47 A. Braun and J. Tcherniac, *J. Ann. Ber.*, 1907, **40**, 2709.
48 H. Von der Weid and E. Diesbach, *Helv. Chim. Acta*, 1927, **10**, 886.
49 N. B. McKeown and N. B. McKeown, *Phthalocyanine Materials: Synthesis, Structure and Function*, Cambridge University Press, Cambridge, UK, 1998, vol. 1.
50 A. L. Thomas, *Phthalocyanine Research and Applications*, CRC Press, 1990.
51 A. G. Dandridge, H. A. E. Drescher and J. Thomas, *In Dyes*, 1929, 169.
52 J. M. Robertson, *J. Chem. Soc.*, 1935, 615.
53 J. M. Robertson, *J. Chem. Soc.*, 1936, 1195.
54 R. P. Linstead and J. M. Robertson, *J. Chem. Soc.*, 1936, 1736.
55 J. M. Robertson and I. D. A. Woodward, *J. Chem. Soc.*, 1937, 219.
56 J. M. Robertson and I. Woodward, *J. Chem. Soc.*, 1940, 36.
57 R. P. Linstead, *J. Chem. Soc.*, 1934, 1016.
58 G. T. Byrne, R. P. Linstead and A. R. Lowe, *J. Chem. Soc.*, 1934, 1017.
59 C. E. Dent and R. P. Linstead, *J. Chem. Soc.*, 1934, 1027.
60 C. E. Dent, R. P. Linstead and A. R. Lowe, *J. Chem. Soc.*, 1934, 1033.
61 D. Gounden, N. Nombona and W. E. van Zyl, *Coord. Chem. Rev.*, 2020, **420**, 213359.
62 S. Yang, Y. Yu, X. Gao, Z. Zhang and F. Wang, *Chem. Soc. Rev.*, 2021, **50**, 12985.
63 D. Li, S. Cai, P. Wang, H. Cheng, B. Cheng, Y. Zhang and G. Liu, *Adv. Healthc. Mater.*, 2023, **12**, 2300263.

64 T. Furuyama, K. Satoh, T. Kushiya and N. Kobayashi, *J. Am. Chem. Soc.*, 2014, **136**, 765.
65 H. Tomoda, E. Hibiya, T. Nakamura, H. Ito and S. Saito, *Chem. Lett.*, 1976, **5**, 1003.
66 T. Haruhiko, S. Shojiro, O. Shojiro and S. Shinsaku, *Chem. Lett.*, 2006, **9**, 1277.
67 S. W. Oliver and T. D. Smith, *J. Chem. Soc., Perkin Trans. 2*, 1987, 1579.
68 P. J. Brach, S. J. Grammatica, O. A. Ossanna and L. Weinberger, *J. Heterocycl. Chem.*, 1970, **7**, 1403.
69 H. J. Callot, F. Metz and C. Piechocki, *Tetrahedron*, 1982, **38**, 2365.
70 G. de la Torre, G. Bottari, U. Hahn and T. Torres, in *Functional Phthalocyanine Molecular Materials*, 2010, pp. 1–44.
71 C. C. Leznoff, M. Hu and K. J. M. Nolan, *Chem. Commun.*, 1996, 1245.
72 J. Follana-Berná, R. Farran, W. Leibl, A. Quaranta, Á. Sastre-Santos and A. Aukauloo, *Angew. Chem., Int. Ed.*, 2021, **60**, 12284.
73 O. L. Kaliya, E. A. Lukyanets and G. N. Vorozhtsov, *J. Porphyrins Phthalocyanines*, 1999, **3**, 592.
74 B. A. Bench, W. W. Brennessel, H.-J. Lee, S. M. Gorun, H. Ali and J. E. van Lier, *Angew. Chem. Int. Ed.*, 2002, **41**, 747.
75 O. Tsaryova, A. Semioshkin, D. Wöhrle and V. I. Bregadze, *J. Porphyrins Phthalocyanines*, 2012, **9**, 268.
76 X. Duan, Y. Zhang, H. Wang, F. Dai, G. Yang and Y. Chen, *New J. Chem.*, 2020, **44**, 13240.
77 C. P. S. Ribeiro and L. L. M. O. Lourenço, *J. Photochem. Photobiol.*, 2021, **48**, 1.
78 S. R. D. Gamelas, A. T. P. C. Gomes, M. A. F. Faustino, A. C. Tomé, J. P. C. Tomé, A. Almeida and L. M. O. Lourenço, *ACS Appl. Bio Mater.*, 2020, **3**, 4044.
79 L. M. O. Lourenço, D. M. G. C. Rocha, C. I. V. Ramos, M. C. Gomes, A. Almeida, M. A. F. Faustino, F. A. Almeida Paz, M. Neves, A. Cunha, J. P. C. Tome, L. M. O. Lourenço, Deisy, M. G. C. Rocha, C. I. V. Ramos, M. C. Gomes, M. A. F. Faustino, F. A. Almeida Paz, M. G. P. M. S. Neves, Â. Cunha and J. P. C. Tomé, *ChemPhotoChem*, 2019, **3**, 251.
80 L. M. O. Lourenço, A. Sousa, M. C. Gomes, M. A. F. Faustino, A. Almeida, A. M. S. Silva, M. G. P. M. S. Neves, J. A. S. Cavaleiro, Â. Cunha and J. P. C. Tomé, *Photochem. Photobiol. Sci.*, 2015, **14**, 1853.
81 K. A. D. F. Castro, J. A. Prandini and L. M. O. Lourenço, *Front. Chem.*, 2022, **10**, 1.
82 L. M. O. Lourenço, P. M. R. Pereira, E. Maciel, M. Válega, F. M. J. Domingues, M. R. M. Domingues, M. G. P. M. S. Neves, J. A. S. Cavaleiro, R. Fernandes and J. P. C. Tomé, *Chem. Commun.*, 2014, **50**, 8363.
83 L. M. O. Lourenço, M. G. P. M. S. Neves, J. A. S. Cavaleiro and J. P. C. Tomé, *Tetrahedron*, 2014, **70**, 2681.
84 J. Lopes-Nunes, J. Carvalho, J. Figueiredo, C. I. V. Ramos, L. M. O. Lourenço, J. P. C. Tomé, M. G. P. M. S. Neves, J. L. Mergny, J. A. Queiroz, G. F. Salgado and C. Cruz, *Bioorg. Chem.*, 2020, **100**, 103920.
85 C. I. V. Ramos, S. P. Almeida, L. M. O. Lourenço, P. M. R. Pereira, R. Fernandes, M. A. F. Faustino, J. P. C. Tomé, J. Carvalho, C. Cruz and M. G. P. M. S. Neves, *Molecules*, 2019, **24**, 733.
86 L. M. O. Lourenço, B. A. Iglesias, P. M. R. Pereira, H. Girão, R. Fernandes, M. G. P. M. S. Neves, J. A. S. Cavaleiro and J. P. C. Tomé, *Dalton Trans.*, 2015, **44**, 530.
87 S. Dutta, B. G. Ongarora, H. Li, M. G. H. da Vicente, B. K. Kolli and K. P. Chang, *PLoS One*, 2011, **6**, e20786.
88 J. M. D. Calmeiro, J. P. C. Tomé and L. M. O. Lourenço, *J. Mater. Chem. C*, 2020, **8**, 8344.
89 L. Wibmer, L. M. O. Lourenço, A. Roth, G. Katsukis, M. G. P. M. S. Neves, J. A. S. Cavaleiro, J. P. C. Tomé, T. Torres and D. M. Guldi, *Nanoscale*, 2015, **7**, 5674.
90 L. M. O. Lourenço, A. Hausmann, C. Schubert, M. G. P. M. S. Neves, J. A. S. Cavaleiro, T. Torres, D. M. Guldi and J. P. C. Tomé, *ChemPlusChem*, 2015, **80**, 832.
91 L. C. Nene and T. Nyokong, *Diamond Relat. Mater.*, 2023, **131**, 109549.
92 B. Uprety and H. Abrahamse, *Front. Chem.*, 2022, **10**, 946574.
93 L. Lei, B. Dai, T. Han, C. Zhou, Z. Gong and P. Zhang, *Front. Mater.*, 2022, **9**, 744.
94 X. Xu, R. Ray, Y. Gu, H. J. Ploehn, L. Gearheart, K. Raker and W. A. Scrivens, *J. Am. Chem. Soc.*, 2004, **126**, 12736.
95 C. Xia, S. Zhu, T. Feng, M. Yang, B. Yang, C. Xia, T. Feng, M. Yang, B. Yang and S. Zhu, *Adv. Sci.*, 2019, **6**, 1901316.
96 D. Yakovlev, E. Kolesova, S. Sizova, K. Annas, M. Tretyak, V. Loschenov, A. Orlova and V. Oleinikov, *Nanomaterials*, 2022, **12**, 3874.
97 A. C. S. Samia, X. Chen and C. Burda, *J. Am. Chem. Soc.*, 2003, **125**, 15736.
98 Ş. Eryiğit, A. Gelir, E. Budak, C. Ünlü, A. Gömleksiz, İ. Özçeşmeci and A. Gül, *Luminescence*, 2022, **37**, 268.
99 L. Fan, Y. Hu, X. Wang, L. Zhang, F. Li, D. Han, Z. Li, Q. Zhang, Z. Wang and L. Niu, *Talanta*, 2012, **101**, 192.
100 O. J. Achadu, I. Uddin and T. Nyokong, *J Photochem Photobio A: Chem*, 2016, **317**, 12.
101 I. Scalise and E. N. Durantini, *Bioorg. Med. Chem.*, 2005, **13**, 3037.
102 M. K. Nazeeruddin, R. Humphry-Baker, M. Grätzel, M. K. Nazeeruddin, R. Humphry-Baker, M. Grätzel and B. A. Murrer, *Chem. Commun.*, 1998, **6**, 719.
103 O. J. Achadu and T. Nyokong, *New J. Chem.*, 2016, **40**, 8727.
104 S. E. Korkut, D. Akyüz, K. Özdoıan, Y. Yerli, A. Koca and M. K. Şener, *Dalton Trans.*, 2016, **45**, 3086.
105 O. J. Achadu and T. Nyokong, *J. Fluoresc.*, 2016, **26**, 283.
106 O. J. Achadu and T. Nyokong, *Talanta*, 2017, **166**, 15.
107 O. J. Achadu and T. Nyokong, *Dyes Pigm.*, 2017, **145**, 189.
108 A. M. Santiago, C. I. M. Santos, L. M. O. Lourenço, I. F. A. Mariz, J. P. C. Tomé and E. Maçôas, *Nanomaterials*, 2022, **12**, 1892.

109 O. J. Achadu and T. Nyokong, *Dyes Pigm.*, 2019, **160**, 328.
110 A. Ogunsipe, J. Y. Chen and T. Nyokong, *New J. Chem.*, 2004, **28**, 822.
111 O. J. Achadu and T. Nyokong, *Dyes Pigm.*, 2019, **160**, 328.
112 W. Jiang, M. Jiang, T. Wang, X. Chen, M. Zeng, J. Yang, Z. Zhou, N. Hu, Y. Su and Z. Yang, *RSC Adv.*, 2021, **11**, 14805.
113 W. Jiang, X. Chen, T. Wang, B. Li, M. Zeng, J. Yang, N. Hu, Y. Su, Z. Zhou and Z. Yang, *RSC Adv.*, 2021, **11**, 5618.
114 S. M. Mousavi, M. Y. Kalashgrani, N. Javanmardi, M. Riazi, M. H. Akmal, V. Rahmanian, A. Gholami and W. H. Chiang, *J. Mater. Chem. B*, 2024, **12**, 7041.
115 A. Karagianni, N. G. Tsierkezos, M. Prato, M. Terrones and K. V. Kordatos, *Carbon*, 2023, **203**, 273.
116 R. Matshitse, K. E. Sekhosana, O. J. Achadu and T. Nyokong, *J. Coord. Chem.*, 2017, **70**, 3308.
117 T. Fan, W. Zeng, W. Tang, C. Yuan, S. Tong, K. Cai, Y. Liu, W. Huang, Y. Min and A. J. Epstein, *Nanoscale Res. Lett.*, 2015, **10**, 1.
118 N. Nwahara, R. Nkhahle, B. P. Ngoy, J. Mack and T. Nyokong, *New J. Chem.*, 2018, **42**, 6051.
119 L. C. Nene, M. E. Managa, D. O. Oluwole, D. M. Mafukidze, A. Sindelo and T. Nyokong, *Inorg. Chim. Acta*, 2019, **488**, 304.
120 L. C. Nene, M. Managa and T. Nyokong, *Dyes Pigm.*, 2019, **165**, 488.
121 L. C. Nene and T. Nyokong, *Photodiagn. Photodyn. Ther.*, 2021, **36**, 102573.
122 K. Celep, G. Gökçil, P. Şen, F. Şahin, A. Erdoğmuş and G. Y. Atmaca, *Appl. Organomet. Chem.*, 2025, **39**, e70007.
123 G. Gökçil, G. Y. Atmaca, P. Şen, F. Şahin and A. Erdoğmuş, *J. Photochem. Photobiol., A*, 2025, **459**, 116108.
124 G. Gökçil, K. Celep, P. Şen, F. Şahin, A. Erdoğmuş and G. Y. Atmaca, *Polyhedron*, 2025, **272**, 117468.
125 R. Matshitse and T. Nyokong, *J. Fluoresc.*, 2018, **28**, 827.
126 R. Matshitse, N. Nwaji, M. Mananga, E. Prinsloo and T. Nyokong, *J. Photochem. Photobiol., A*, 2018, **367**, 253.
127 M. De, S. Ghosh, T. Sen, M. Shadab, I. Banerjee, S. Basu and N. Ali, *Mol. Ther. – Nucleic Acids*, 2018, **10**, 9.
128 G. van der Horst, A. F. van de Merbel, E. Ruigrok, M. H. van der Mark, E. Ploeg, L. Appelman, S. Tvingsholm, M. Jäätelä, J. van Uhm, M. Kruithof-de Julio, G. N. Thalmann, R. C. M. Pelger, C. H. Bangma, J. L. Boormans, G. van der Pluijm and E. C. Zwarthoff, *Mol. Oncol.*, 2020, **14**, 3121.
129 Y. I. Openda, P. Sen, M. Managa and T. Nyokong, *Photodiagn. Photodyn. Ther.*, 2020, **29**, 101607.
130 L. Hui, J. Huang, G. Chen, Y. Zhu and L. Yang, *ACS Appl. Mater. Interfaces*, 2016, **8**, 20.
131 P. M. Sivakumar, G. Sheshayan and M. Doble, *Chem. Biol. Drug Des.*, 2008, **72**, 303.
132 P. Sen, N. Nwahara and T. Nyokong, *Main Group Chem.*, 2021, **20**, 175.
133 M. Özçeşmeci, S. Gümrükçü, C. Ünlü, İ.Y Coşkun, S. Özdemir, M. S. Yalçın, G. Tollu and İ. Özçeşmeci, *Appl. Organomet. Chem.*, 2024, **38**, e7423.
134 D. M. Mafukidze and T. Nyokong, *J. Coord. Chem.*, 2017, **70**, 3598.
135 O. J. Achadu, M. Managa and T. Nyokong, *J. Photochem. Photobiol., A*, 2017, **C**, 174.
136 Q. Chen, Y. Liu, B. Mao, Z. Wu, W. Yan, D. Zhang, Q. Li, H. Huang, Z. Kang and W. Shi, *Adv. Funct. Mater.*, 2023, **33**, 2305318.
137 S. A. Majeed, N. Nwaji, J. Mack, T. Nyokong and S. Makhseed, *J. Lumin.*, 2019, **213**, 88.
138 D. AlMarzouq, S. A. Majeed, Ö. Budak and A. Koca, *Inorg. Chim. Acta*, 2021, **527**, 120558.
139 M. Cacioppo, T. Scharl, L. Đorđević, A. Cadranel, F. Arcudi, D. M. Guldi and M. Prato, *Angew. Chem., Int. Ed.*, 2020, **59**, 12779.
140 D. M. Mafukidze and T. Nyokong, *J. Mol. Struct.*, 2019, **1180**, 307.
141 S. Centane, E. K. Sekhosana, R. Matshitse and T. Nyokong, *J. Electroanal. Chem.*, 2018, **820**, 146.
142 C. Luhana, I. Moyo, K. Tshenkeng and P. Mashazi, *Microchem. J.*, 2022, **180**, 107605.
143 H. M. Sharma, D. K. Das and A. Kumar, *Int. J. Hydrogen Energy*, 2024, **110**, 159.
144 K. H. Koh, S. H. Noh, T. H. Kim, W. J. Lee, S. C. Yi and T. H. Han, *RSC Adv.*, 2017, **7**, 26113.
145 Y. Lu, Y. Jiang, X. Gao, X. Wang and W. Chen, *J. Am. Chem. Soc.*, 2014, **136**, 11687.